NAVY DEPARTMENT

THE DAVID W. TAYLOR MODEL BASIN

AERODYNAMICS LABORATORY

WASHINGTON 7, D.C.

TEST RESULTS OF A TWO-DIMENSIONAL PLENUM CHAMBER GROUND EFFECT MACHINE OVER A LIQUID SURFACE

by

Anibal Alfredo Tinajero

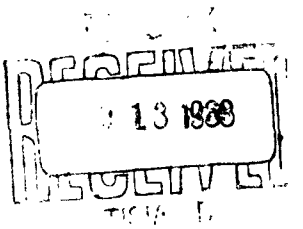

June 1963

FOR ERRATA

AD_____

410027

THE FOLLOWING PAGES ARE CHANGES

TO BASIC DOCUMENT

ERRATA

DAVID TAYLOR MODEL BASIN AERO REPORT 1052

By Anibal Alfredo Tinajero

June 1963

The following changes should be made to the report:

Under "Symbols" delete the last definition.

Page 3: The symbol ρ instead of ρ' should appear in equation (2) and in the line following the equation.

Page 3, last line: The following should be deleted: "(water, in this case)."

Issued 18 July 1963
DTMB - Washington 7, D. C.

NOTATION

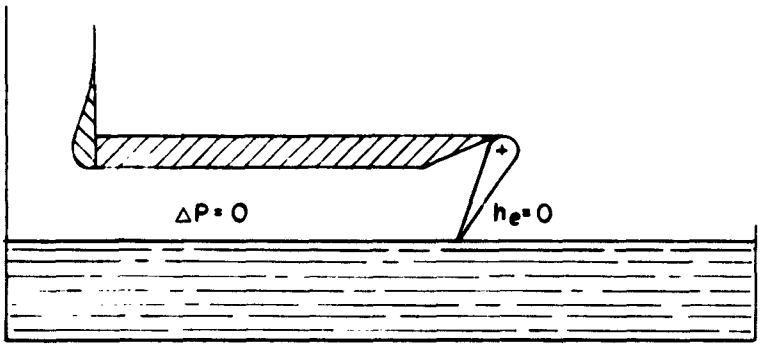
ΔP = 0
h_e = 0

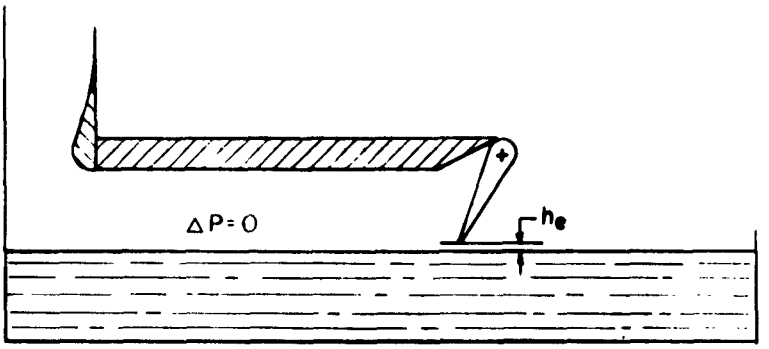
ΔP = 0
h_e

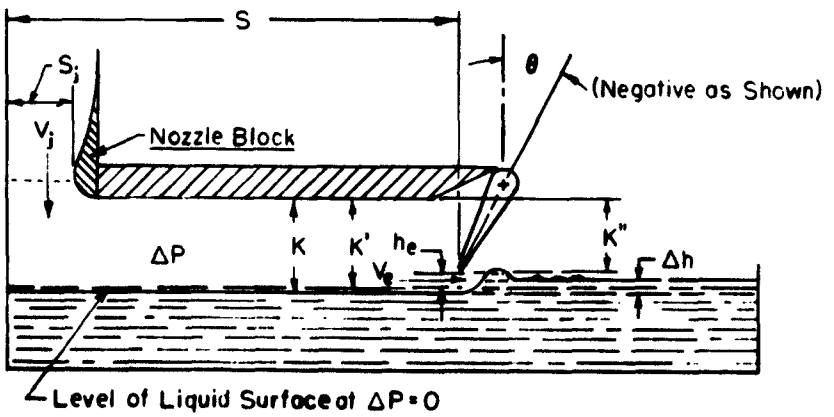
S
S_j
θ
(Negative as Shown)
V_j
Nozzle Block
ΔP
K
K'
h_e
V_e
K"
Δh
Level of Liquid Surface at ΔP = 0

SYMBOLS

a_t	speed of sound in air (a_t = 1117 feet per second)
C	perimeter of flap or skirt (taken at lowest point) in feet
C_p	specific heat at constant pressure in Btu/pound-degree Fahrenheit
C_v	specific heat at constant volume in Btu/pound-degree Fahrenheit
D_c	discharge coefficient
h	height of lowest point of flap or skirt to depressed liquid surface in feet ($h = k - k'' = h_e + \frac{\Delta h}{2}$ for report data only
Δh	amount of liquid surface depression in feet
h_e	height of lowest point of flap or skirt from free liquid surface (when $\Delta h = 0$) in feet
J	jet momentum force in pounds
k	height of model base from depressed surface of liquid in feet ($k = k' + \frac{\Delta h}{2}$ for test)
k'	conc[illegible]ty of model (vertical distance of model base to free su[illegible] of liquid when $\Delta h = 0$) in feet
k''	[illegible]cal distance of model base to lowest point of flap or [illegible]rt in feet ($k'' = k' - h_e$)
P	atmospheric pressure (P = 14.7 pounds per square inch)
ΔP	base pressure in pounds per square foot
P_u	air supply reference pressure in pounds per square inch
Q	rate of flow in cubic feet per second
r	distance from edge of flap to water surface at minimum escape area (see Figure 15)
S	total planform area in square feet
S_i	intake area in square feet
S_e	escape area in square feet ($S_e = Ch$)
V_e	average escape velocity of air at point where S_e is measured, in feet per second
V_i	average airspeed at intake of model in feet per second
V_j	average airspeed at flowmeter throat in feet per second
θ	angle of inclination of flap or skirt in degrees (see notation)
ρ	density of air (ρ = 0.002378 slug per cubic foot)
ρ'	density of water

Aero Report 1052

AERODYNAMICS LABORATORY
DAVID TAYLOR MODEL BASIN
UNITED STATES NAVY
WASHINGTON, D. C.

TEST RESULTS OF A TWO-DIMENSIONAL PLENUM-CHAMBER GROUND EFFECT MACHINE OVER A LIQUID SURFACE

by

Anibal Alfredo Tinajero

SUMMARY

A two-dimensional plenum-chamber GEM with a trailing-edge flap was tested over a liquid surface. The discharge coefficient was determined for the following parameters: ratio of intake to escape area, ratio of planform area to intake area, hover height, planform loading, flap angle, and distance from the trailing edge of the flap to the liquid.

INTRODUCTION

The present investigation was performed to determine the effects of intake area, planform loading, hover height, and flap (or skirt) angle upon the discharge coefficient of a two-dimensional plenum-chamber GEM.

The tests were conducted intermittently in the Aerodynamics Laboratory at the Taylor Model Basin during September and October, 1960. This investigation was carried out in accordance with Reference 1.

MODEL AND TEST EQUIPMENT

The test equipment consisted of a narrow rectangular tank with transparent sides. One end was enclosed with wood; the other was open to allow air to flow freely through a vertical nozzle. For simulation of flight

over a liquid surface, the open end required a barrier to retain the water. A photograph of the test setup is shown in Figure 1.

The model used for representing the GEM consisted of a board with a flap at one end and an inlet diffuser nozzle at the other end. The flap setting could be varied over a wide range of angles, and the size of the inlet was controlled by inserting different nozzle blocks. A photograph of a typical nozzle is shown in Figure 2. Static pressure orifices for determining pressures at the base of the model were located along the length of the board.

CALIBRATION OF FLOWMETER

The calibration of the flowmeter was carried out by measuring the jet force acting upon a modified chemical-type balance, for various values of air supply pressure P_u. A photograph of the flowmeter is shown in Figure 3. The procedure for calibration was to discharge the air through the flowmeter perpendicular to the balance plate. For values of P_u from 10 to 90 psi, the force J on the balance was recorded. The height of the nozzle was that for which the balance would give the highest reading.

The air volume rate of flow, Q, was calculated from the following equation:

$$Q = J/\rho V_j \qquad [1]$$

For several ratios of P/P_u (assuming P = 14.7 psi and the speed of sound a_t = 1117 feet per second), corresponding ratios of V_j/a_t were found in the tables presented in Reference 2 (for $C_p/C_v = 1.4$). For practical purposes, the value of ρ in Equation [1] was assumed constant at 0.002378 slug per cubic foot.

The calibration of the flowmeter, therefore, was in terms of rate of flow for air-supply pressure.

TEST PROCEDURE

Data were obtained at selected ratios of inlet area to model base area, various flap angle settings, ratios of h_e/k', and pressure. The tests were conducted in two phases.

In the first phase (with no air flowing through the flowmeter), the free water surface was barely in contact with the trailing edge of the flap; i.e., h_e was equal to 0. The values for the flap angle θ were varied from -75° to 75° in 15° increments. Then values of Δh were recorded for corresponding values of P_u. The static pressure orifices were utilized to determine whether there was a static pressure gradient along the length of the model and to check the accuracy in the measurement of depth of depression of the water. In a sense, one might look at the model and flow stand as a giant U-tube manometer. Because of the geometry of the model and by definition of h_e, it was necessary to vary the amount of water in the tank in order to maintain the height h_e constant at 0. The same procedure was repeated for each of the inlet nozzle blocks.

For the second phase, h_e was set at some value other than zero. This was done either by adding or evacuating water from the test stand. The values of k' changed automatically with a change in θ, as shown in the notation. The same procedure was repeated for each inlet condition.

RESULTS

The effect of the ratios S_i/S_e, h/k', $\Delta h/h$, h_e/k, and θ upon the discharge coefficient D_c is presented in Figures 4 through 14. The physical meaning of these quantities can be better understood after a careful study of the test setup and the sketch in the notation.

The discharge coefficient D_c was computed from

$$D_c = \frac{Q}{S_e \sqrt{\frac{2\Delta P}{\rho'}}} \qquad [2]$$

where ΔP was obtained from the pressure head, Δh, and ρ' is the density of the fluid (water, in this case).

DISCUSSION

Because of the small size of the test stand and the crude nature of the equipment which was used to obtain the results, the data should be used for preliminary evaluation only. Further testing should be done on a larger scale model, in order to substantiate the results presented herein. For some conditions during the tests it was impossible to obtain data points at the higher values of mass flow, because of an undamped wave-producing oscillation. In some instances (high Δh), the re-enforcement of the oscillation was sufficient to practically evacuate the water from the tank.

A careful study of the data will show that for constant values of k' (with θ constant), if h increases (because of an increase in Δh), the discharge coefficient is decreased. That is, as the planform loading increases, the discharge coefficient decreases. This effect depends on the nature of the flow at the flap trailing edge. To obtain true values of the discharge coefficients for plenum GEM with a flap or skirt, the exhaust area should be computed from

$$S_e = Cr \qquad [3]$$

as shown in Figure 15.

For the test results presented in this report, h was used instead of r, since it was impossible to determine the value of r with sufficient accuracy on a model of such small scale. The value of h was computed from $h = h_e + \frac{\Delta h}{2}$. This was done to simplify testing, since the average position of the flap trailing edge was approximately at the center of the test stand. A slight error due to a small variation in total planform area S occurred for high negative or positive values of θ. Also, blocking of the escape area occurs at high values of planform loading (high value of Δh), because of spillage from the wave generated by the air as it leaves the trailing edge of the flap. For this same configuration, spray is generated by the escaping air travelling in a path tangential to the liquid surface. The amount of spray decreases directly with decrease in Δh, and the nature of the spray was found to vary with θ. This can be readily understood from the sketches in Figure 15. The escaping air

at the trailing edge of the flap is forced to travel through a curved path. The dynamic pressure of the escaping air creates a drop in static pressure (below atmospheric) on the flap surface. Equilibrium is maintained by the wave rise spilling slightly over and toward the flap. As the water spills over, the escaping air pushes against it, generating spray. This situation will be encountered in any GEM when hovering over a liquid surface. For a GEM cruising above "hump speed," the spray will not be generated as in hovering, since $\Delta h = 0$. The amount of lift created in hovering will be equal to the weight of the volume of liquid displaced.

CONCLUSIONS

The results indicate that the discharge coefficient is a function of intake area, flap angle, and planform loading.

The values for discharge coefficients were found to vary considerably with planform loading. Discharge coefficient values should be considered only approximate, because of model size. These results do show a qualitative behavior of a plenum chamber GEM in the over-liquid hovering condition. Further tests, with a larger model, should be carried out to determine the exact contributions of each of the above-mentioned parameters to the discharge coefficients.

Aerodynamics Laboratory
David Taylor Model Basin
Washington, D. C.
May 1963

REFERENCES

1. BUWEPSINST 3920.1 R-12 of 2 Sep 1960
2. Bureau of Naval Weapons. Handbook of Supersonic Aerodynamics. Vol. 2. Wash., Oct 1950. 1 v. (loose-leaf) (NAVORD Rpt. 1488, Vol. 2)

PSD-304,974 (a) Low Planform Loading

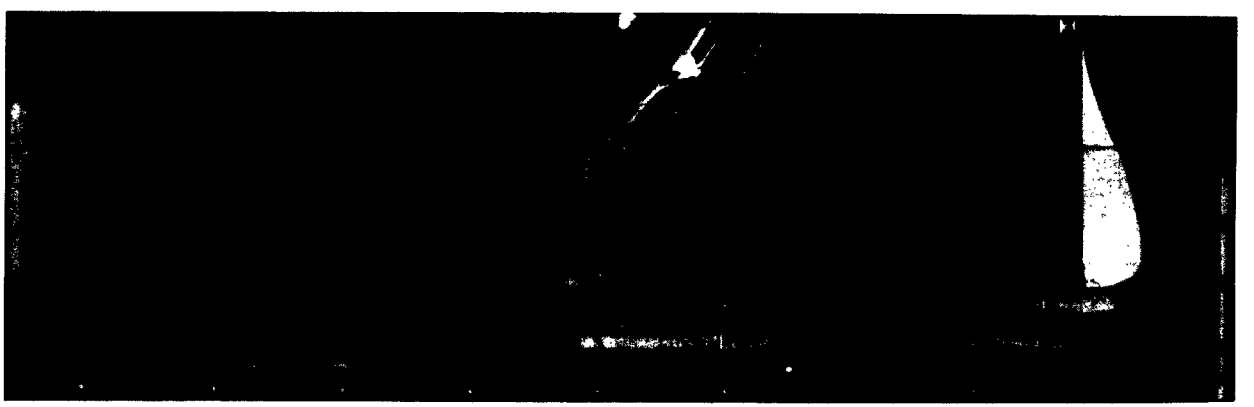

PSD-304,975 (b) High Planform Loading

Figure 1 - Photographs of the Flow Stand

September 11, 1961

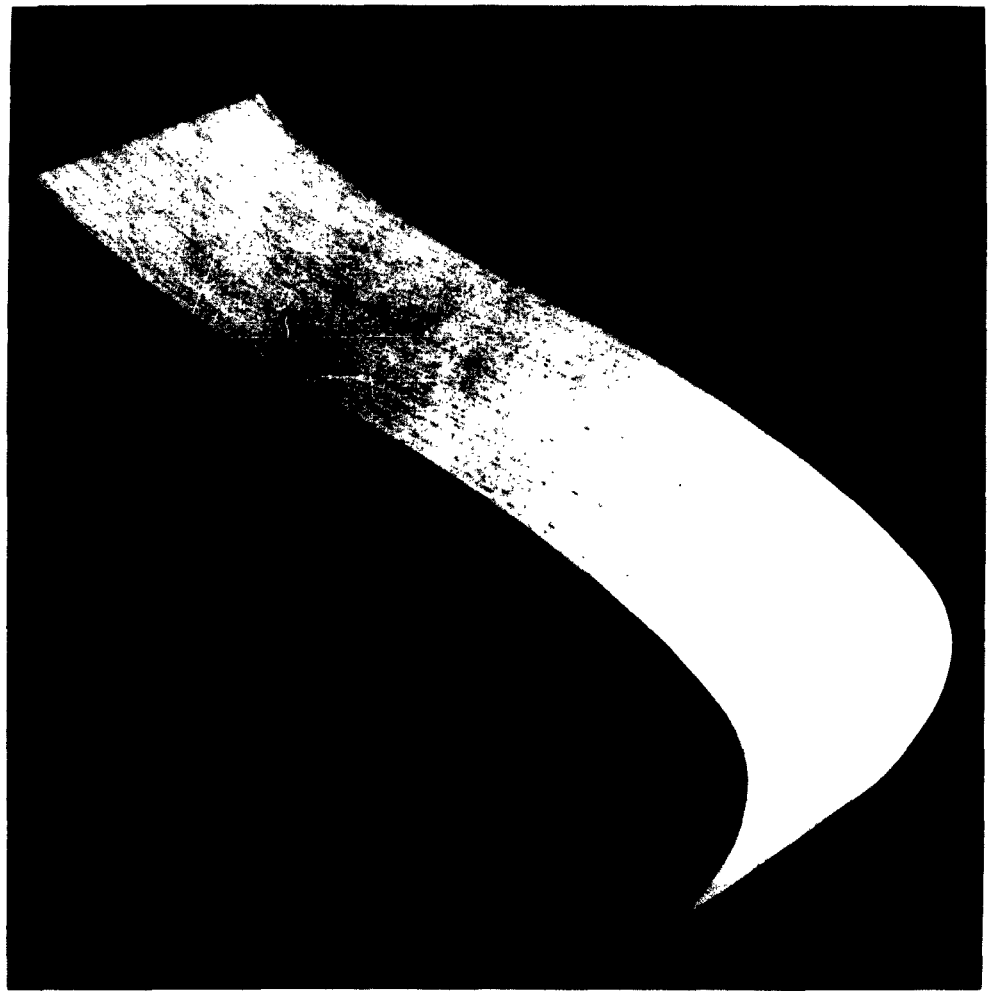

Figure 2 - Photograph of a Typical Intake Nozzle Block

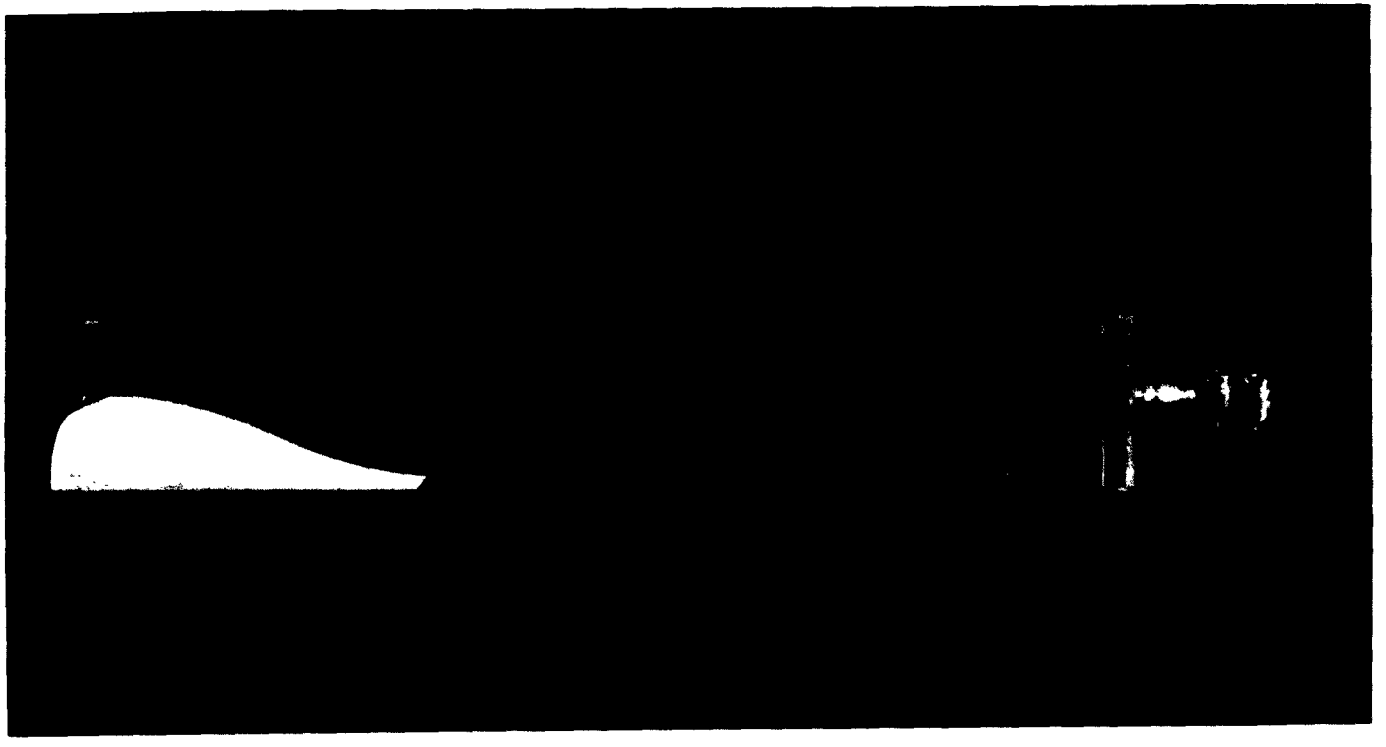

Figure 3 - Photograph of the Flowmeter

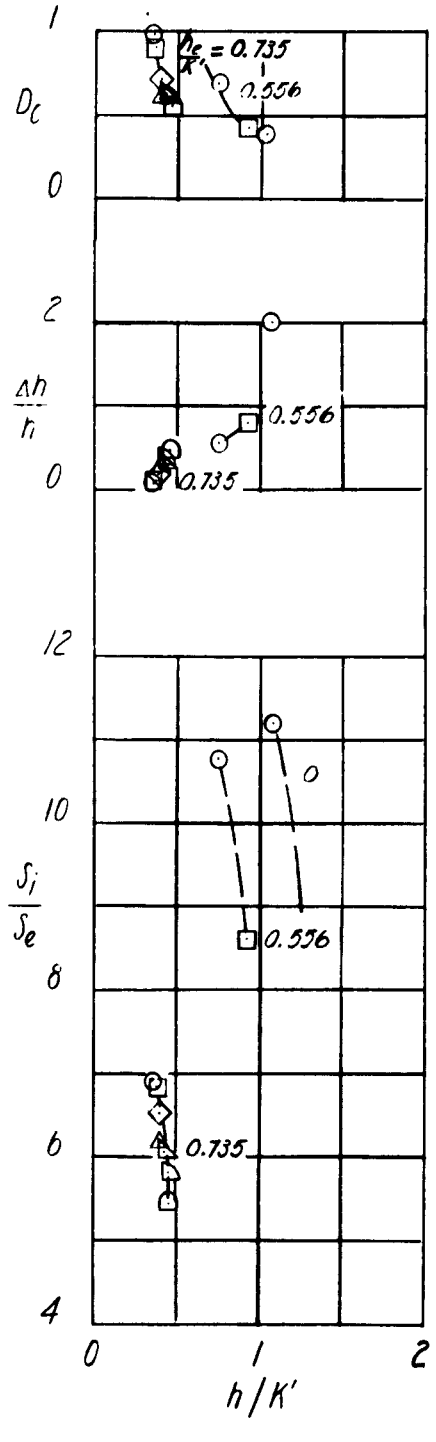

Figure 4 - Variation of the Parameters D_c, $\Delta h/h$, and S_i/S_e With h/k' for Several Values of h_e/k'. $\theta = 75^\circ$

(a) $\frac{S}{S_i} = 6.078$

FIGURE 4a

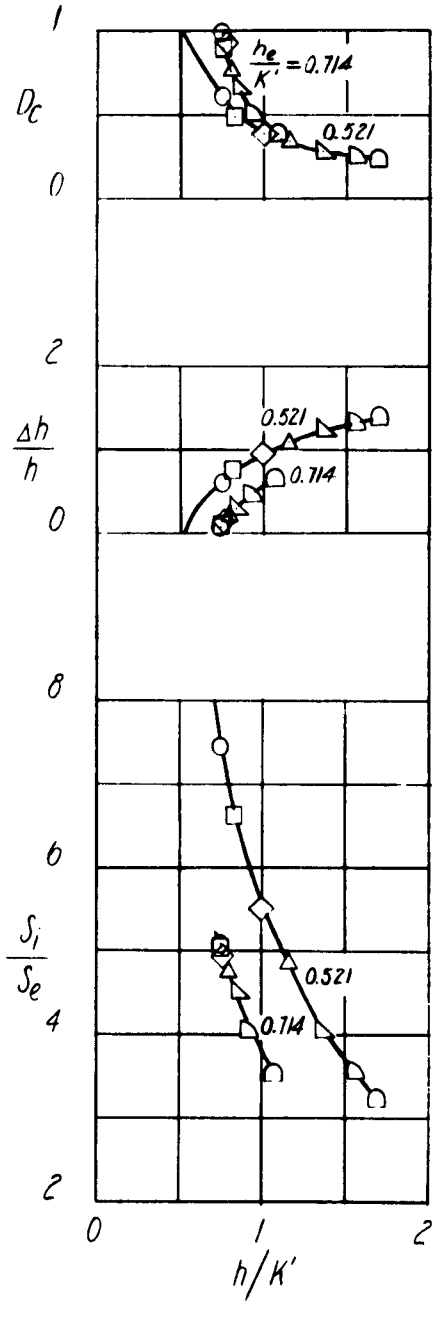

Figure 4 (Continued)
(b) $\frac{S}{S_i} = 8.270$

FIGURE 4b

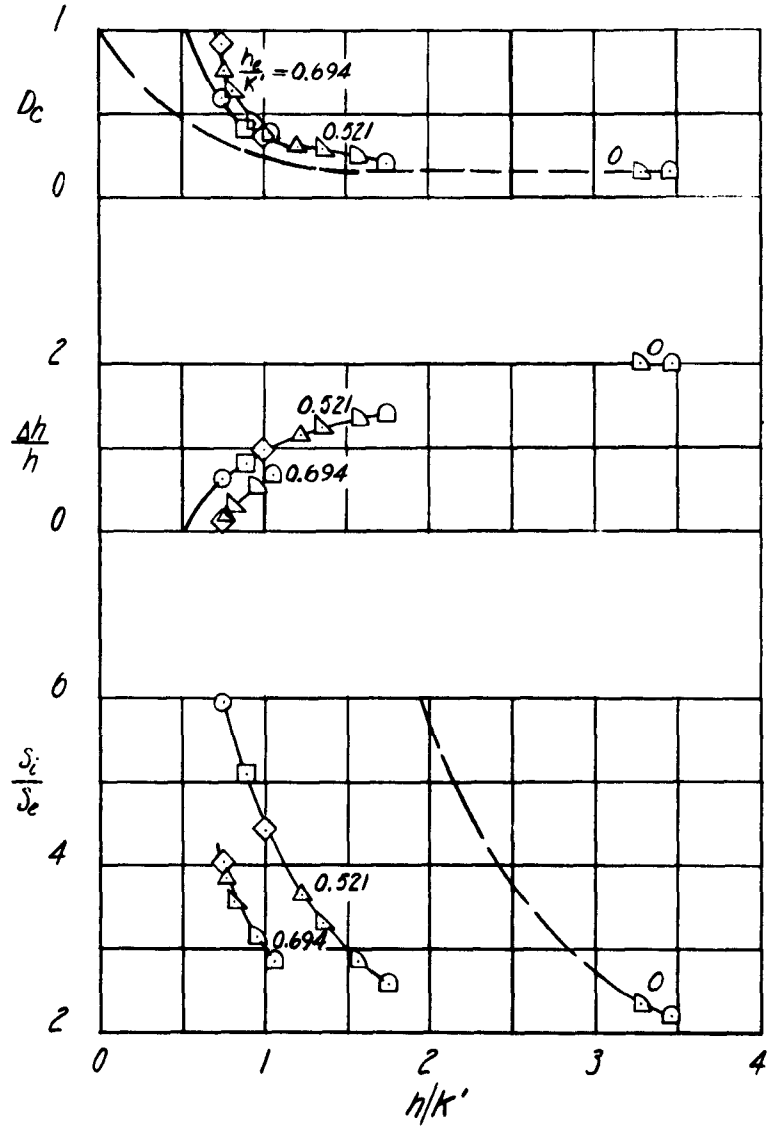

Figure 4 (Continued)
(c) $\frac{S}{S_1} = 10.161$

FIGURE 4c

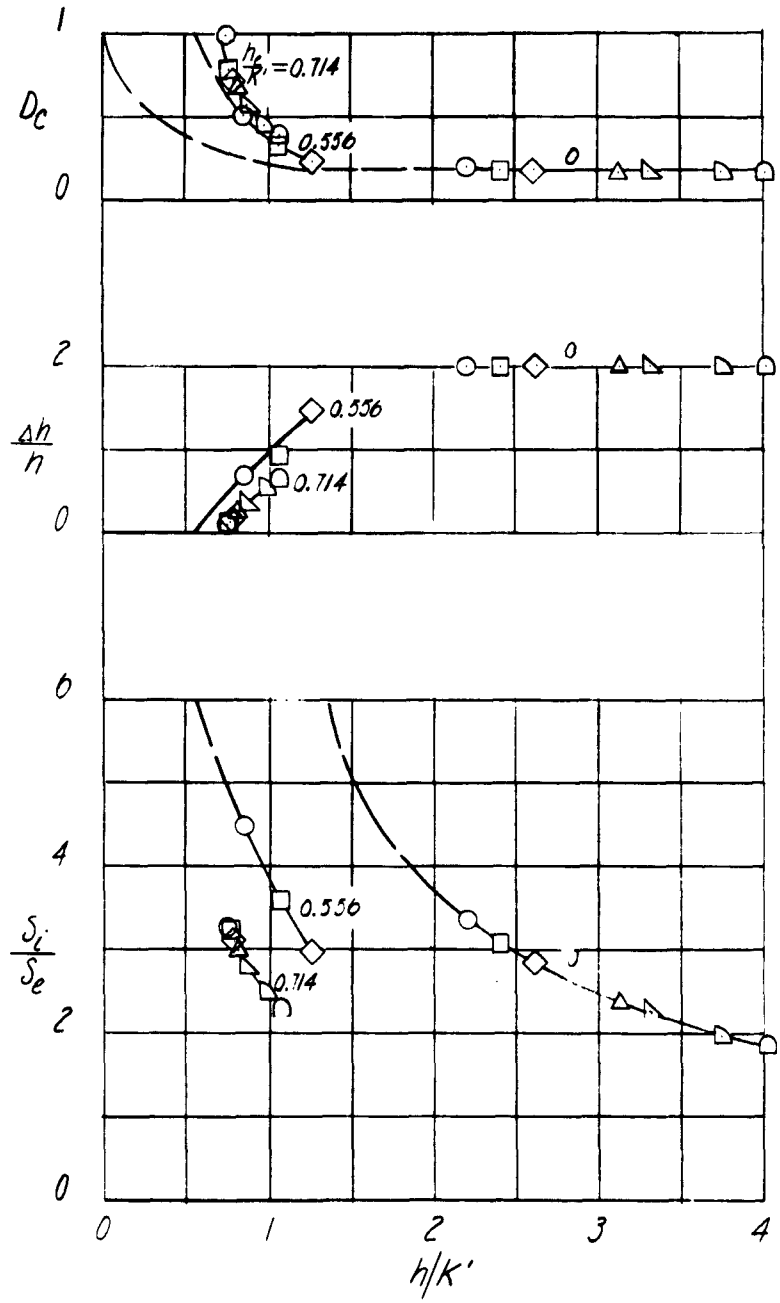

Figure 4 (Continued)

(d) $\frac{S}{S_i} = 12.811$

FIGURE 4d

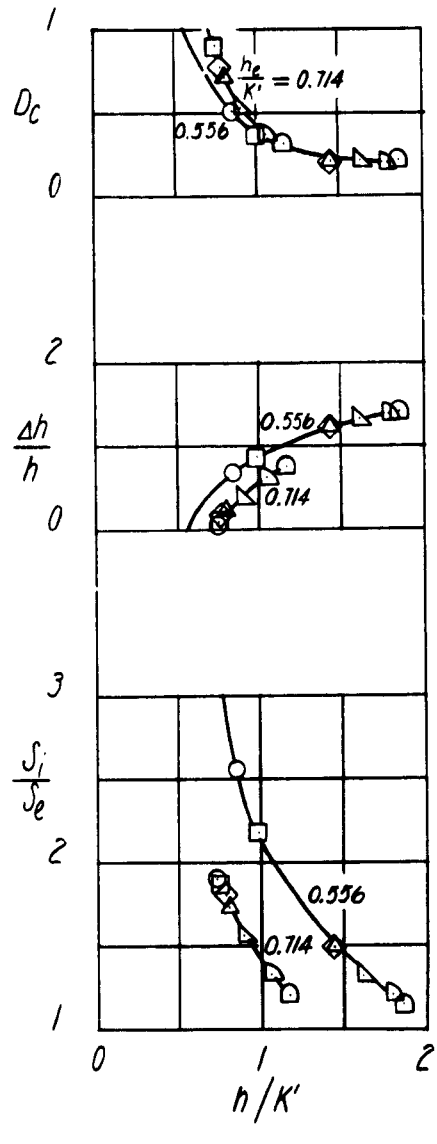

Figure 4 (Continued)
(e) $\frac{S}{S_i}$ = 17.470

FIGURE 4e

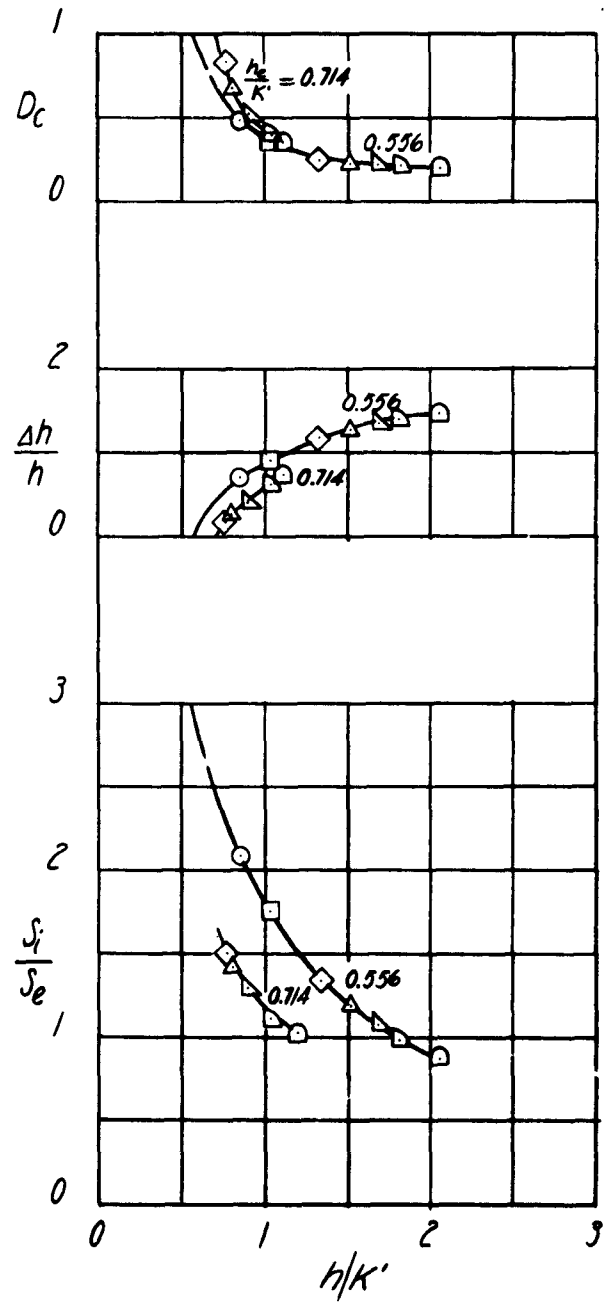

Figure 4 (Concluded)
(f) $\frac{S}{S_1} = 27.111$

FIGURE 4f

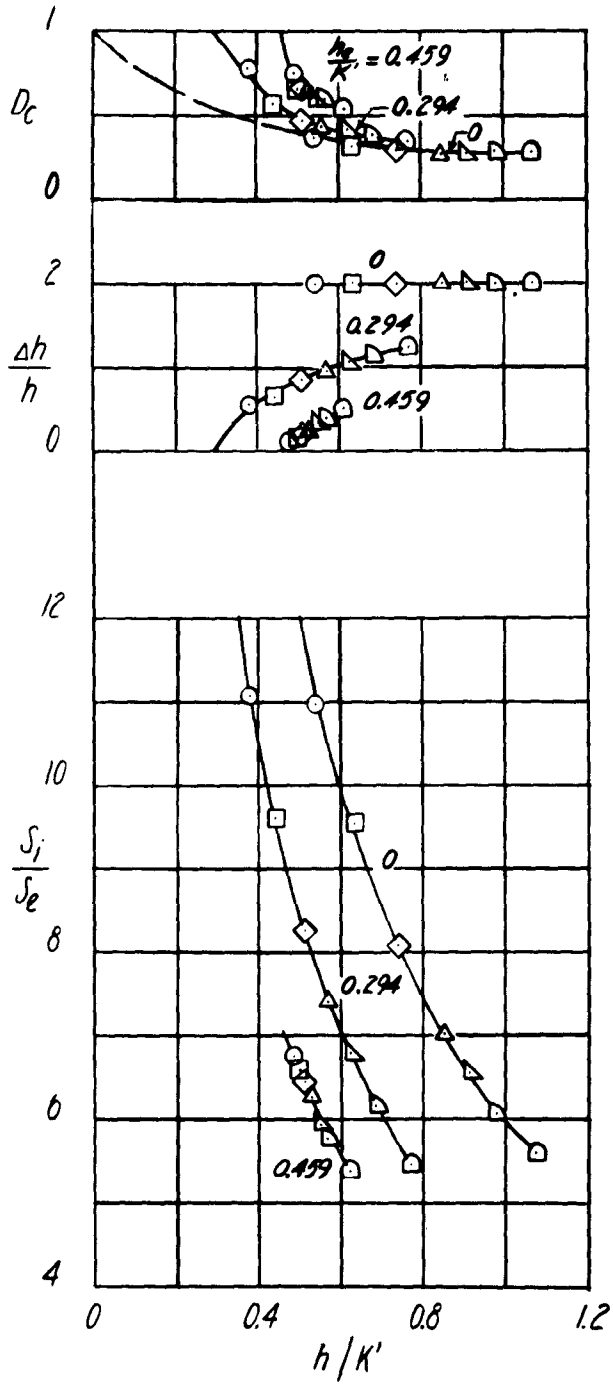

Figure 5 - Variation of the Parameters D_c, $\Delta h/h$, and S_i/S_e With h/k' for Several Values of h_e/k'. $\theta = 60^\circ$

(a) $\frac{S}{S_i} = 6.036$

FIGURE 5a

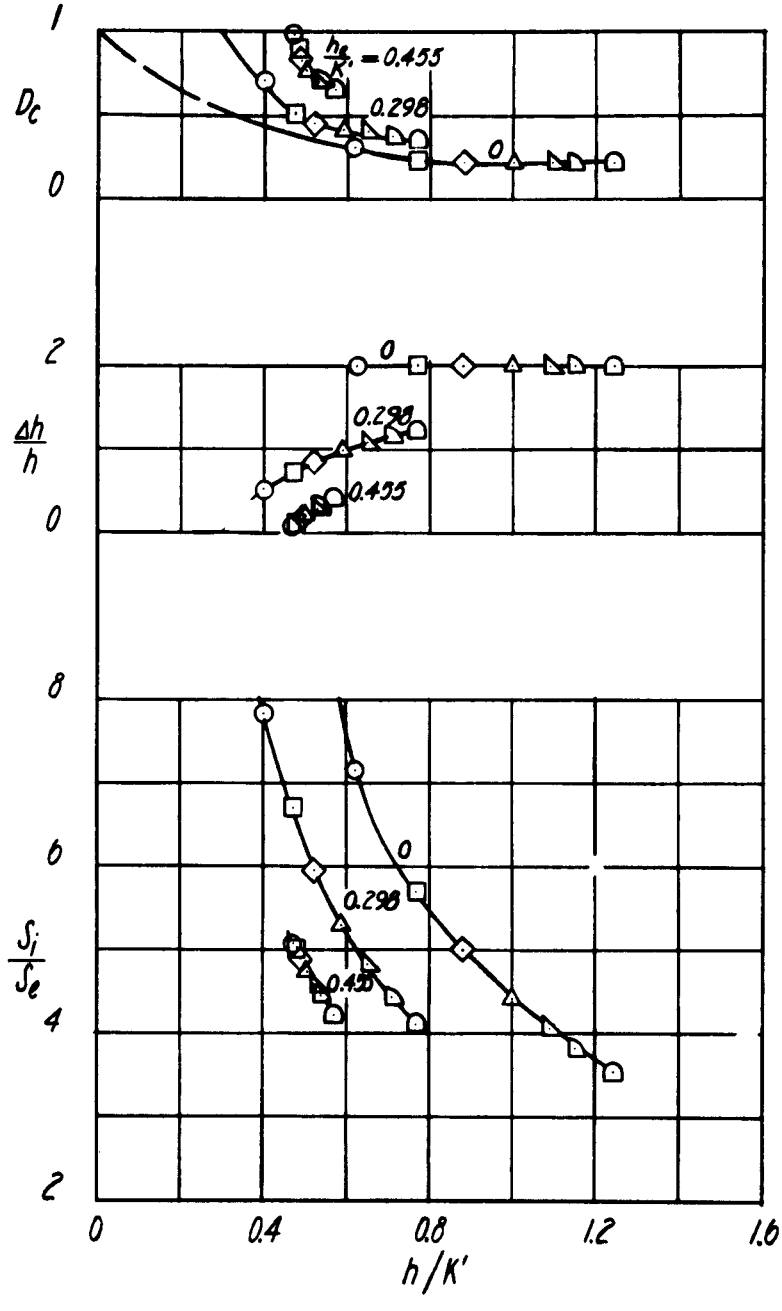

Figure 5 (Continued)

(b) $\frac{S}{S_i}$ = 8.214

FIGURE 5b

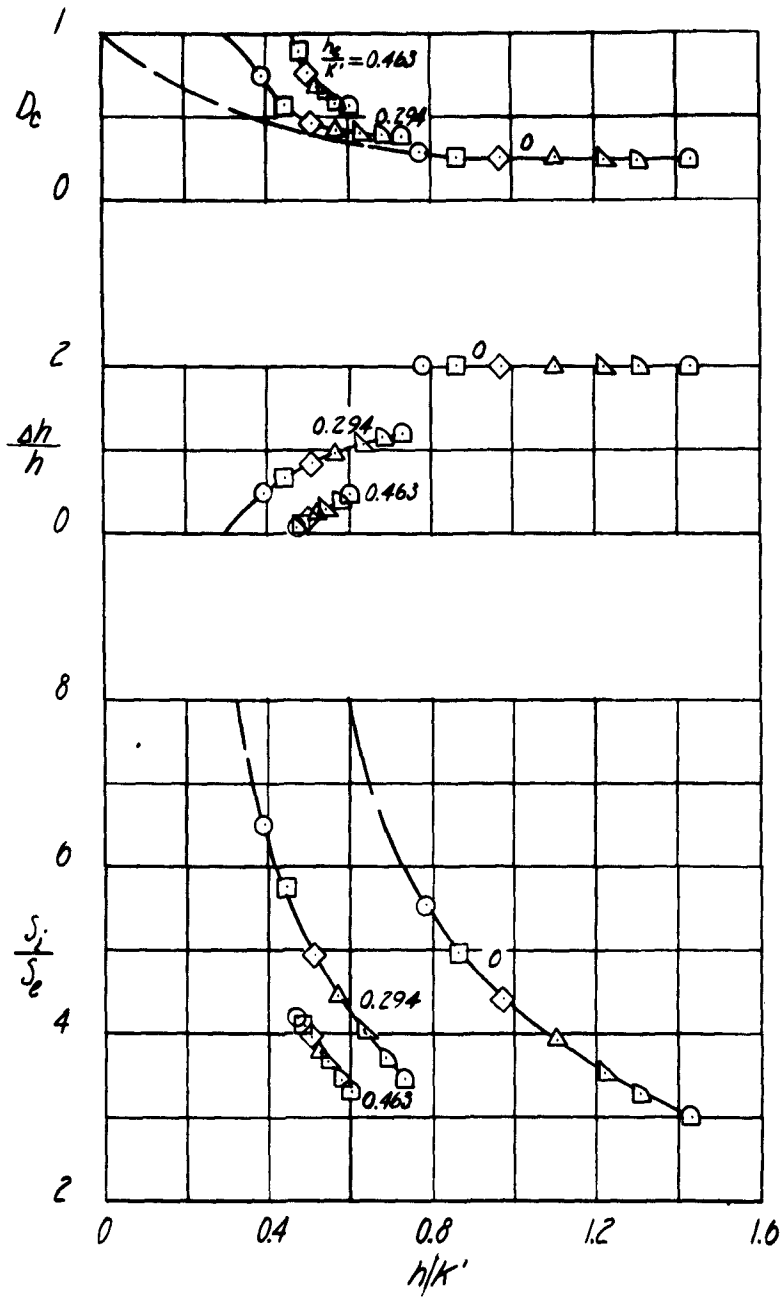

Figure 5 (Continued)
(c) $\frac{S}{S_1}$ = 10.091

FIGURE 5c

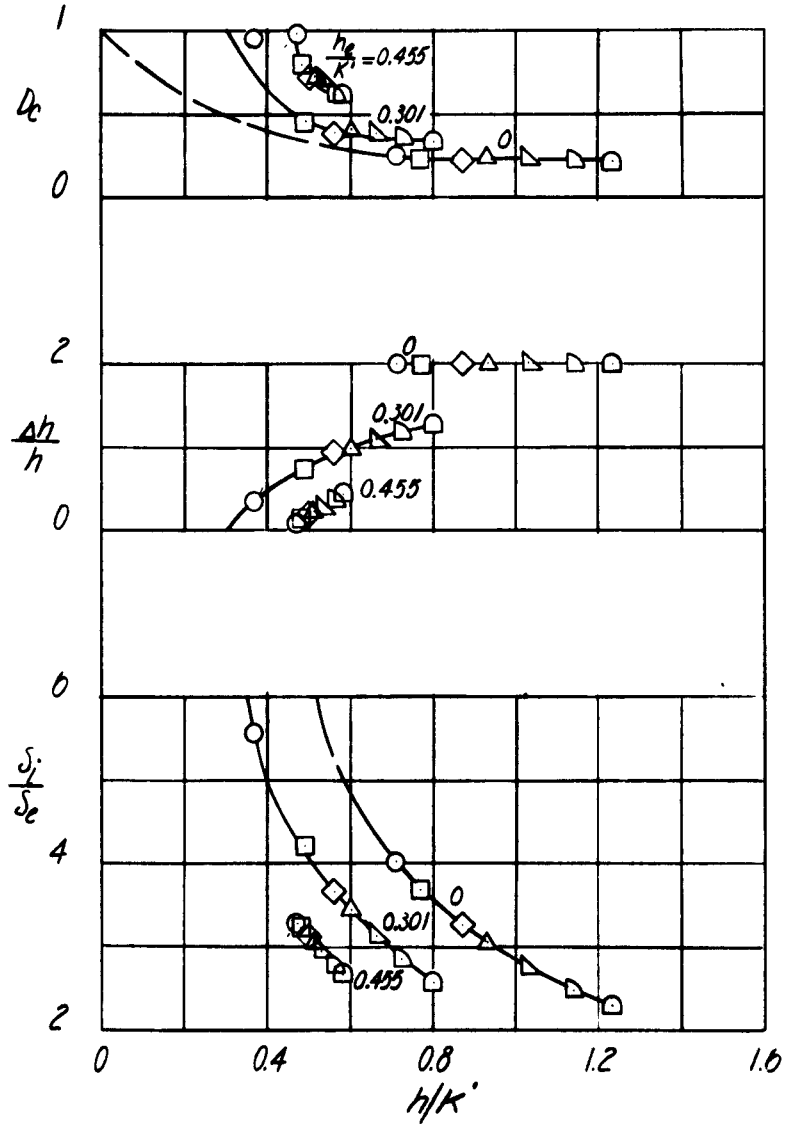

Figure 5 (Continued)
(d) $\frac{S}{S_1}$ = 12.723

FIGURE 5d

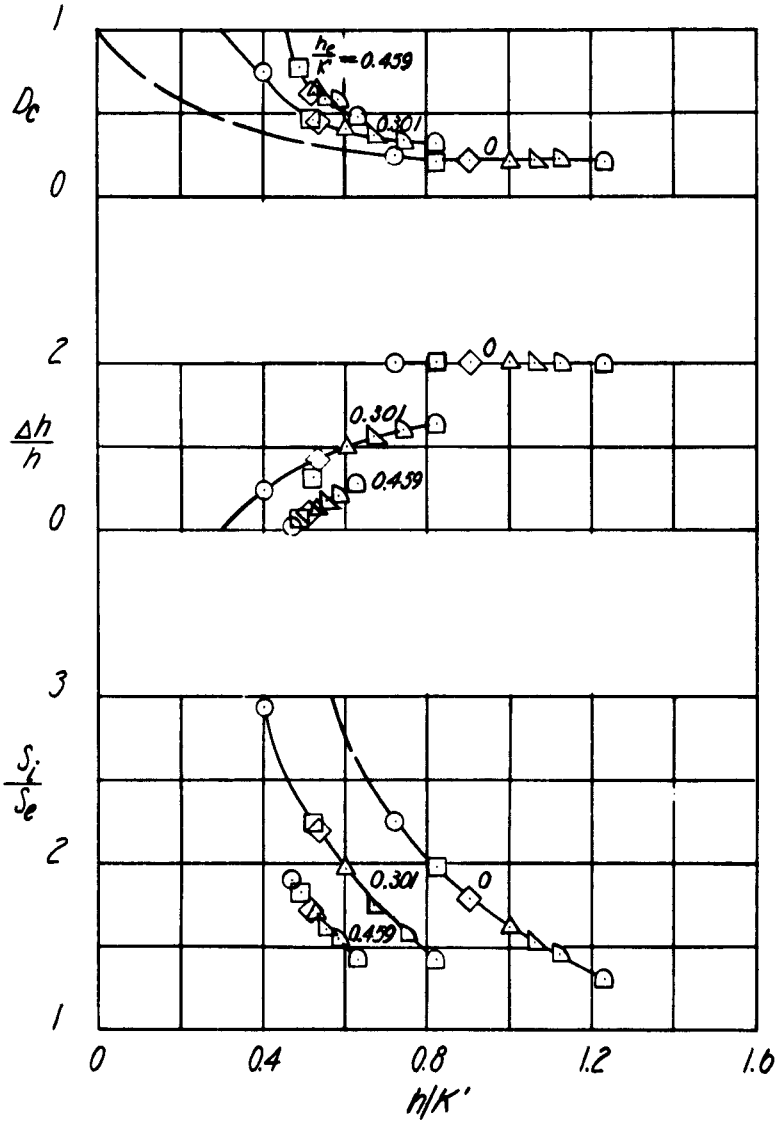

Figure 5 (Continued)
(e) $\frac{S}{S_1} = 17.349$

FIGURE 5e

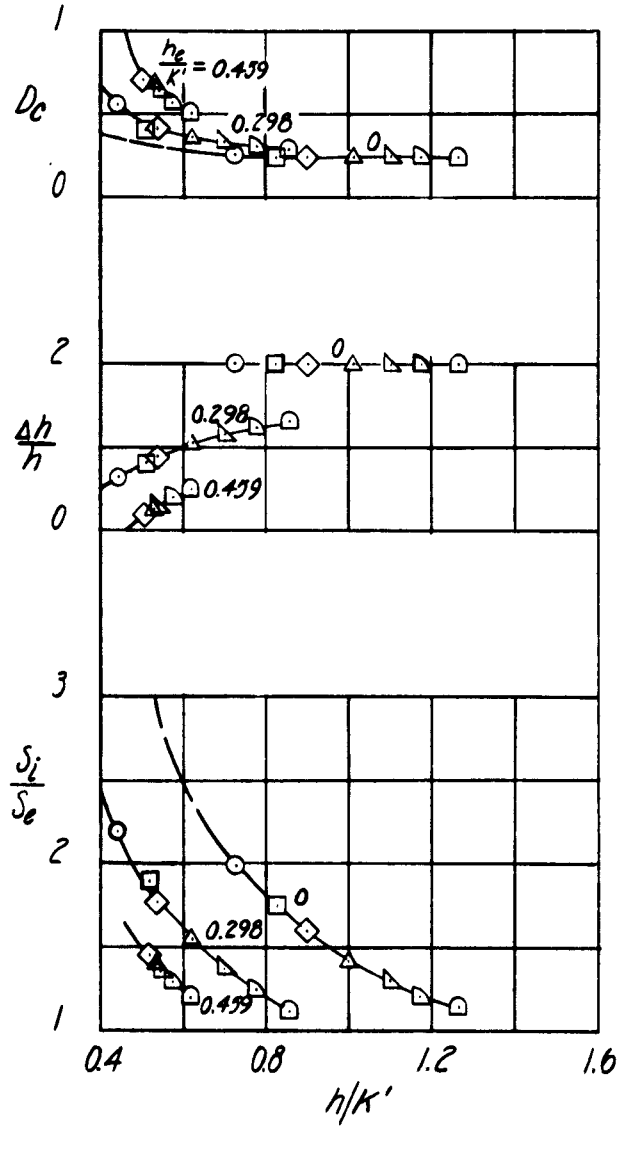

Figure 5 (Concluded)
(f) $\frac{S}{S_1} = 26.924$

FIGURE 5f

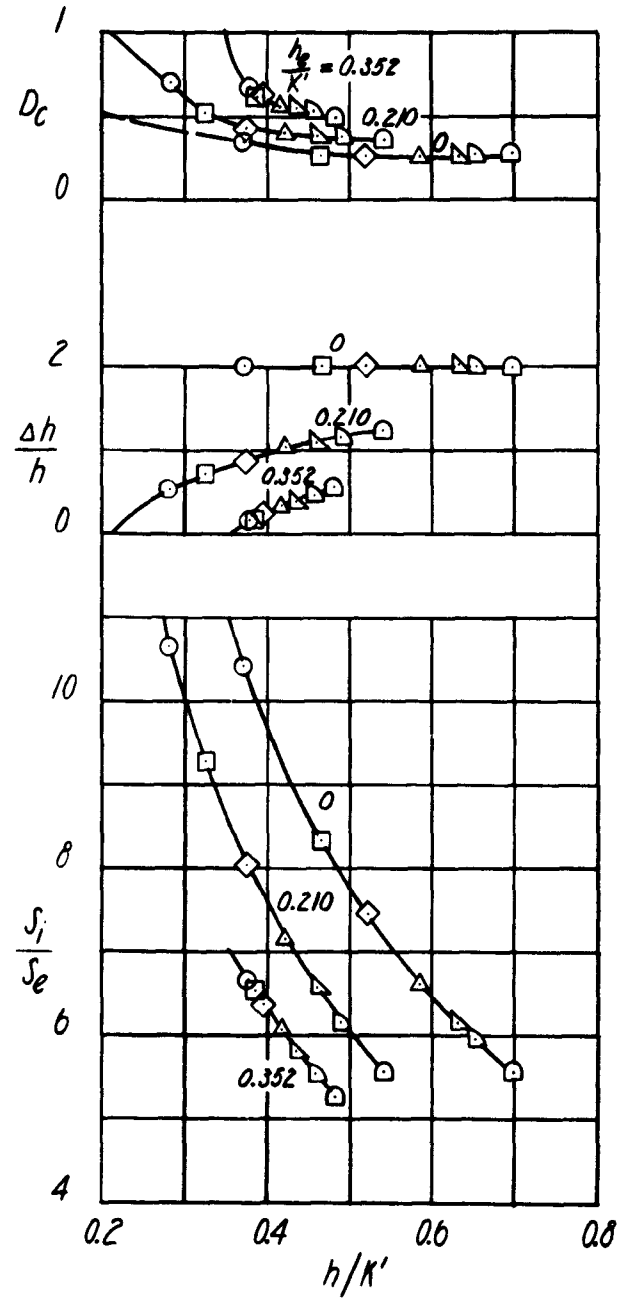

Figure 6 - Variation of the Parameters D_c, $\Delta h/h$, and S_i/S_e With h/k' for Several Values of h_e/k'. $\theta = 45°$

(a) $\frac{S}{S_i} = 5.979$

FIGURE 6a

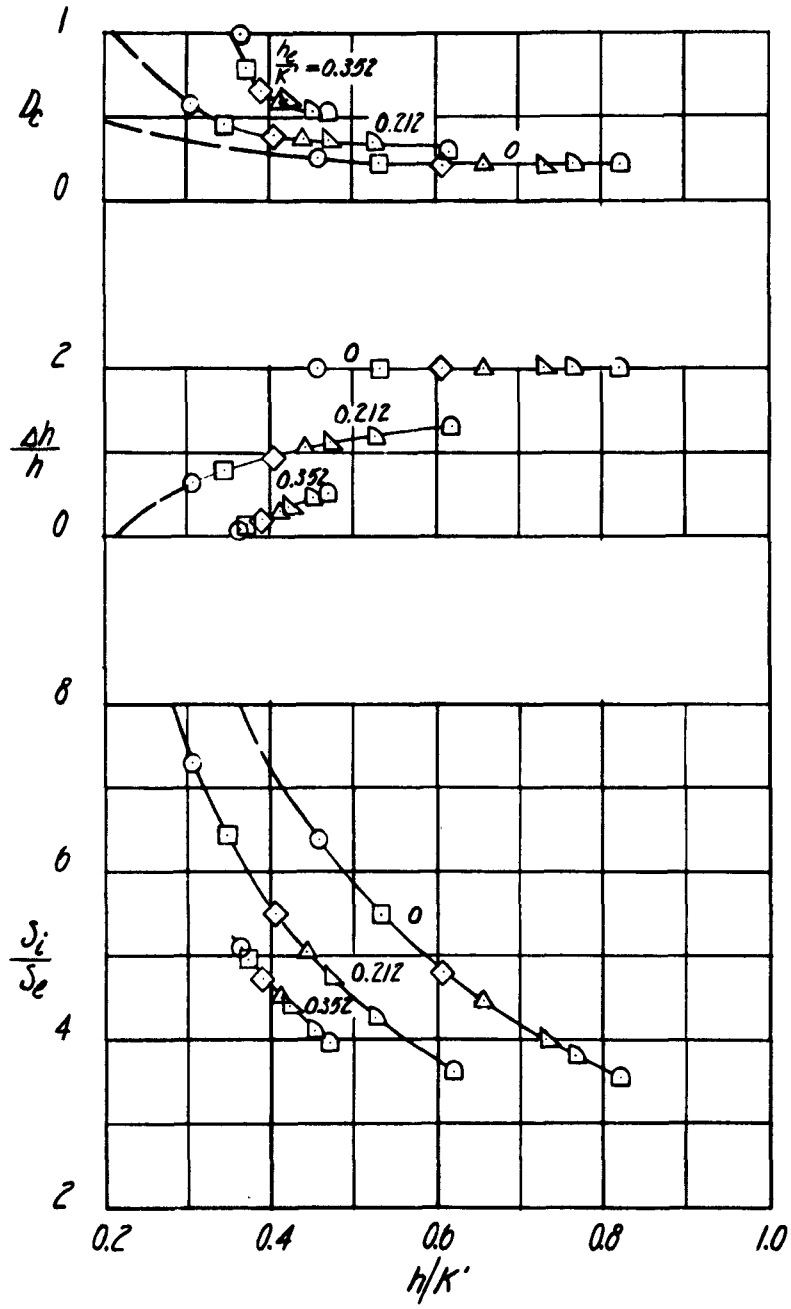

Figure 6 (Continued)

(b) $\frac{S}{S_i}$ = 8.123

FIGURE 6b

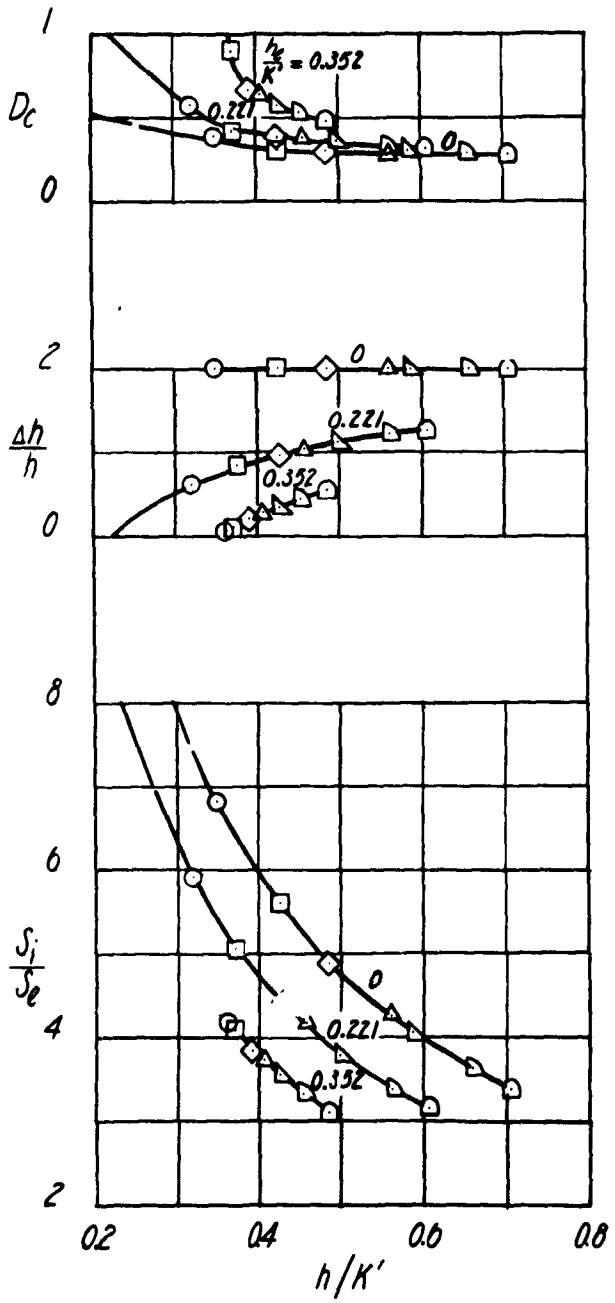

Figure 6 (Continued)
(c) $\frac{S}{S_i}$ = 9.980

FIGURE 6c

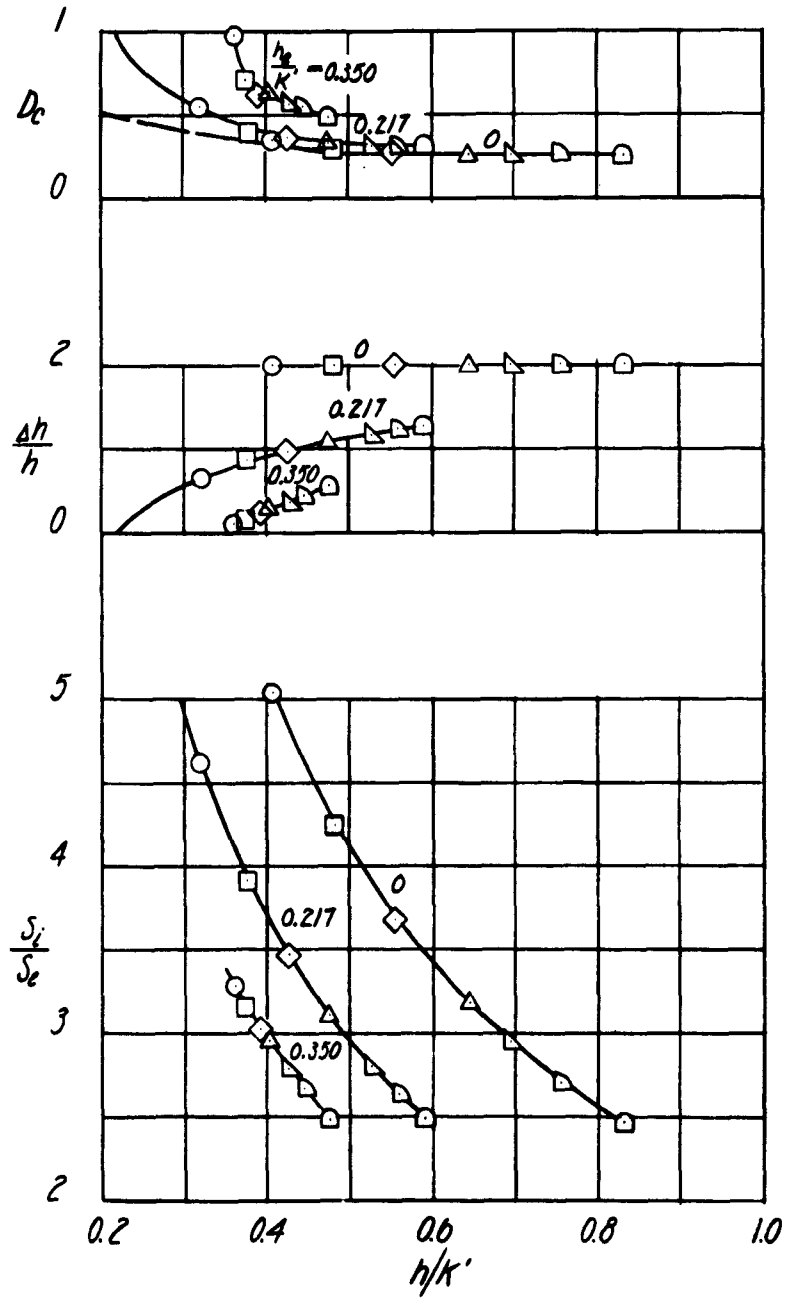

Figure 6 (Continued)

(d) $\frac{S}{S_1}$ = 12.583

FIGURE 6d

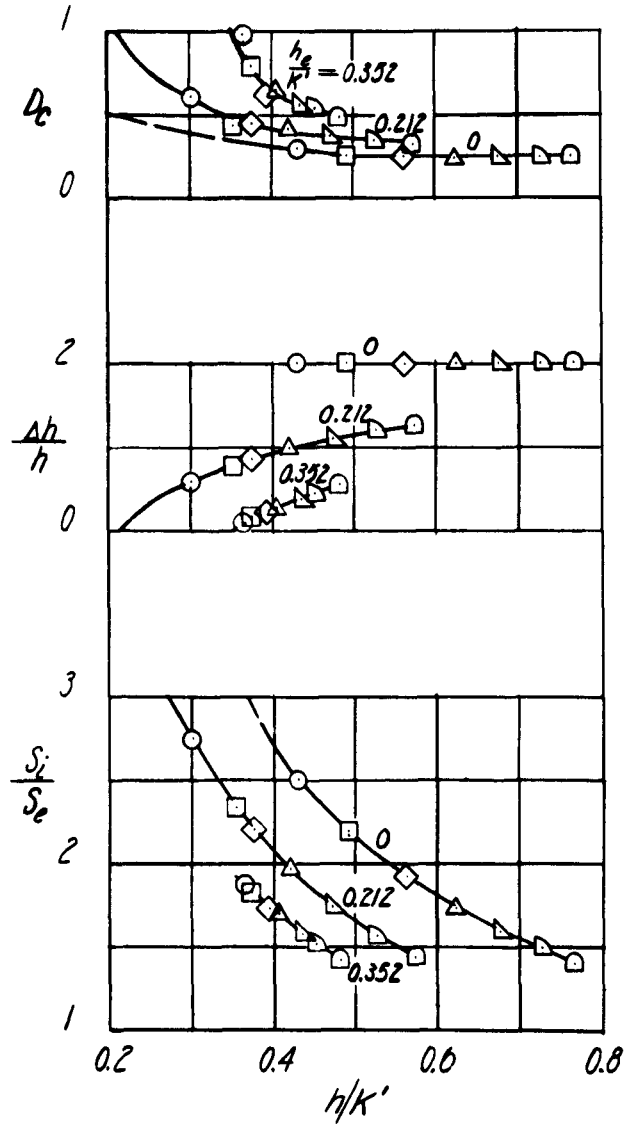

Figure 6 (Continued)
(e) $\frac{S}{S_1} = 17.156$

FIGURE 6e

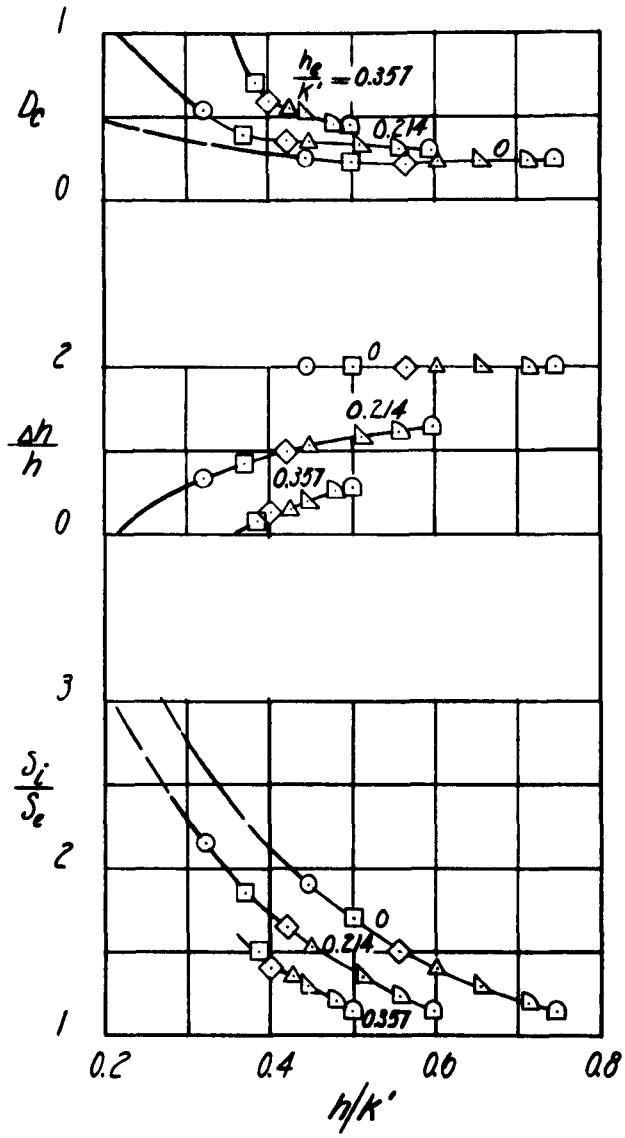

Figure 6 (Concluded)
(f) $\frac{S}{S_1} = 26.623$

FIGURE 6f

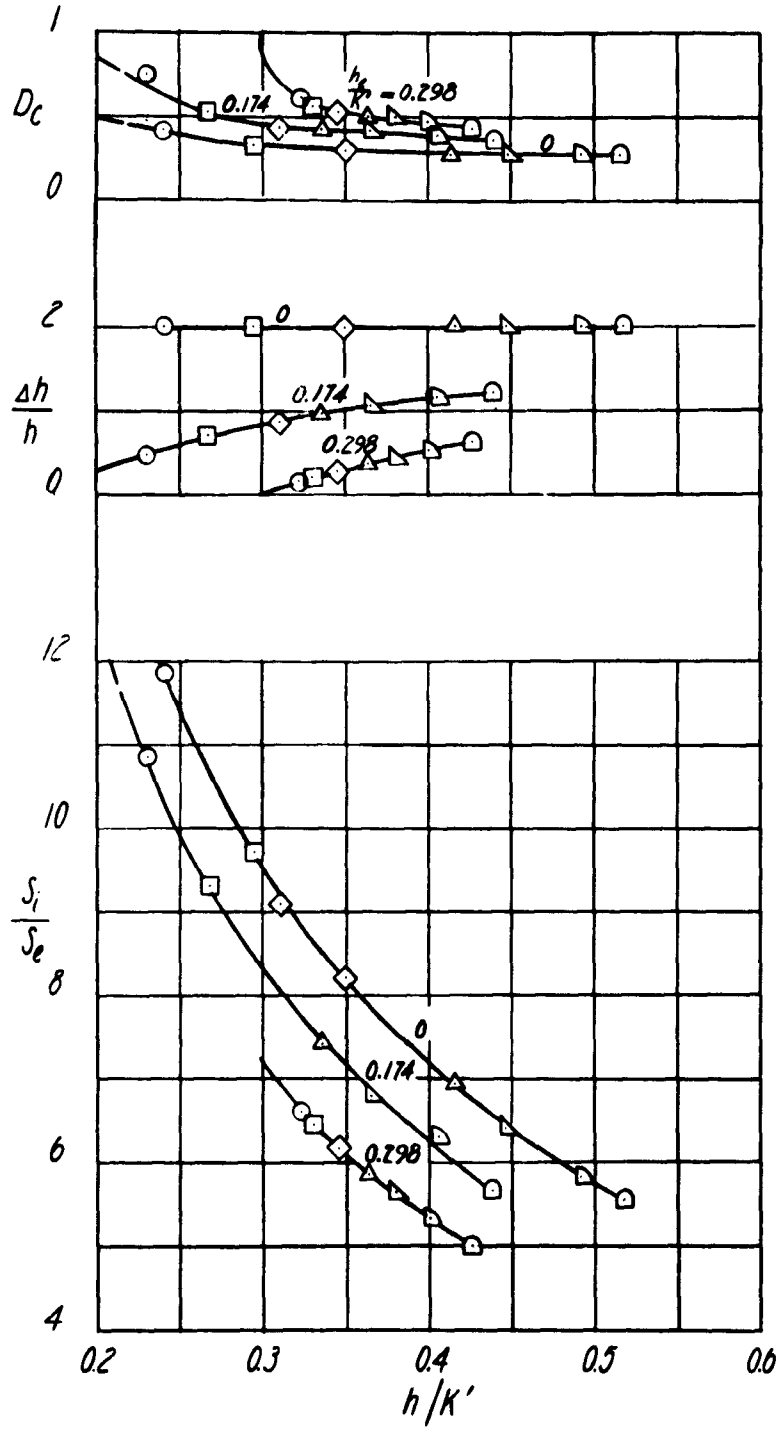

Figure 7 - Variation of the Parameters D_c, $\Delta h/h$, and S_i/S_e With h/k' for Several Values of h_e/k'. $\theta = 30^\circ$

(a) $\frac{S}{S_i} = 5.900$

FIGURE 7a

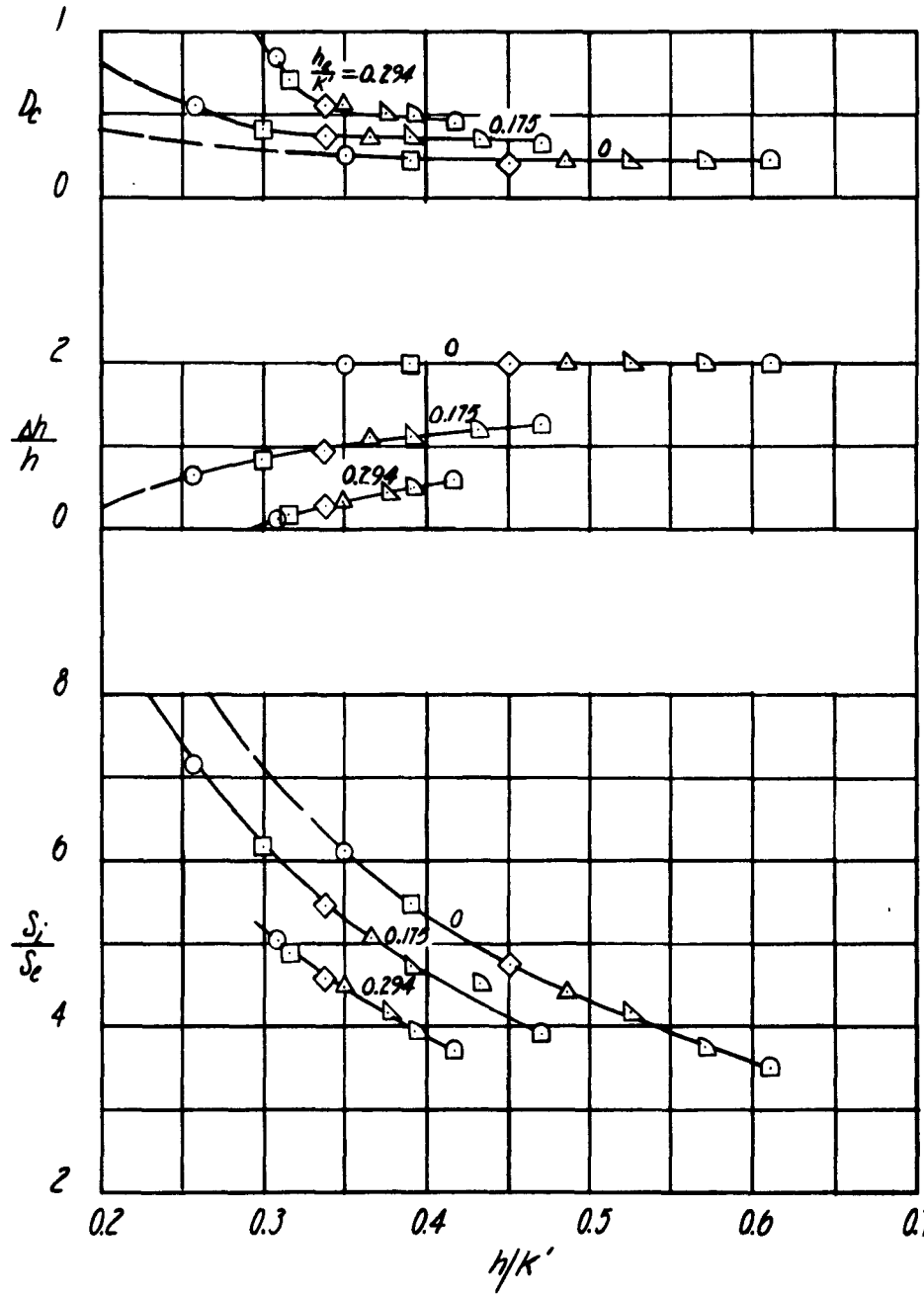

Figure 7 (Continued)
(b) $\frac{S}{S_i}$ = 8.028

FIGURE 7b

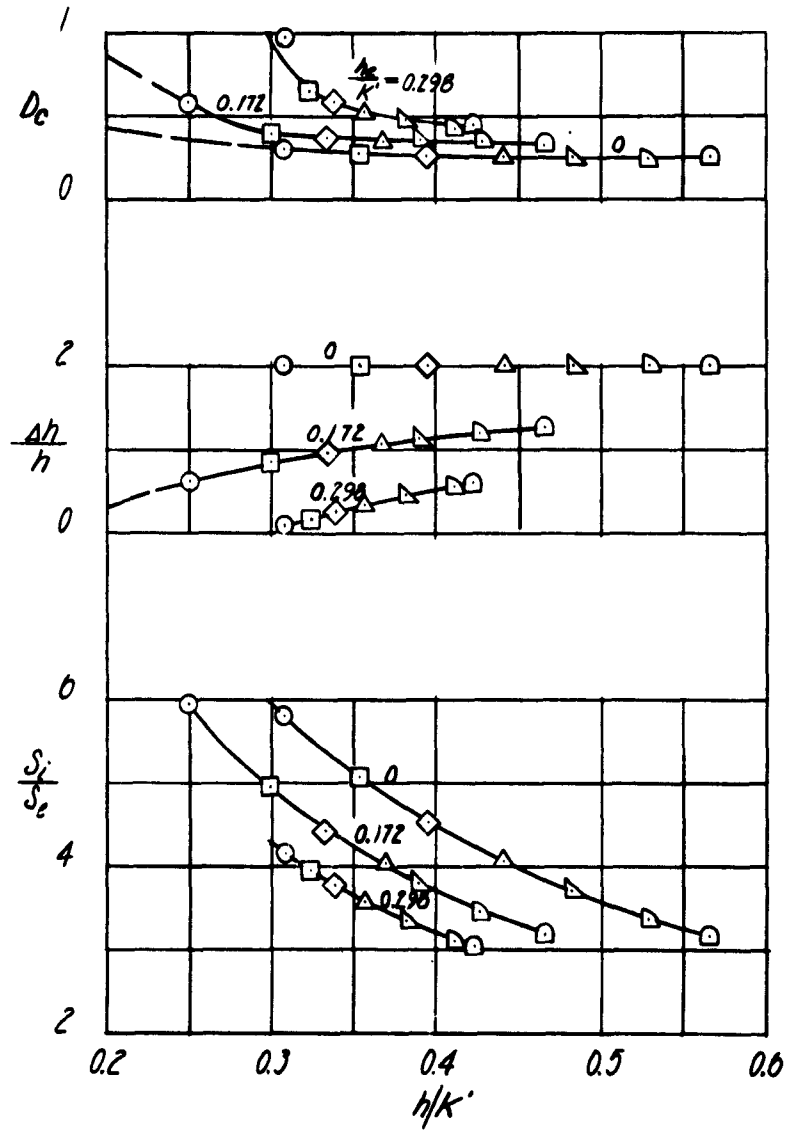

Figure 7 (Continued)
(c) $\frac{S}{S_i}$ = 9.863

FIGURE 7c

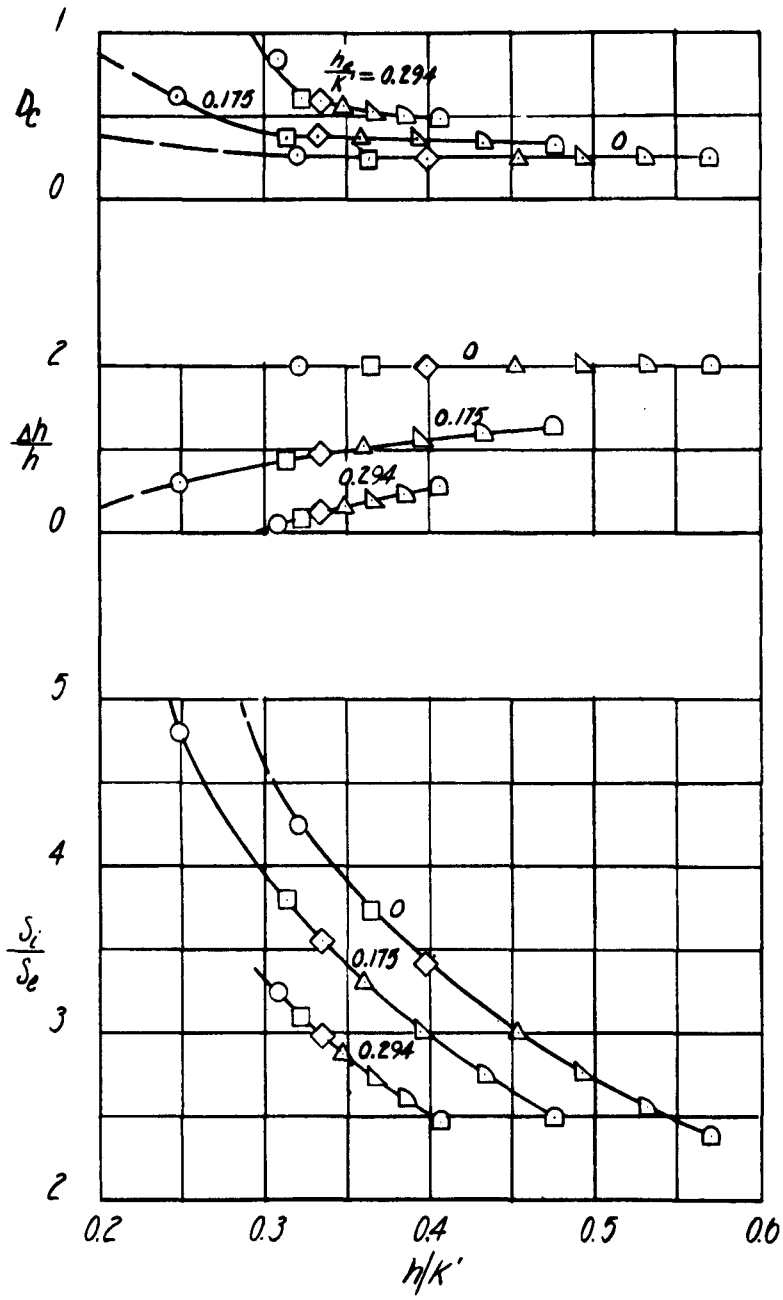

Figure 7 (Continued)
(d) $\frac{S}{S_i} = 12.435$

FIGURE 7d

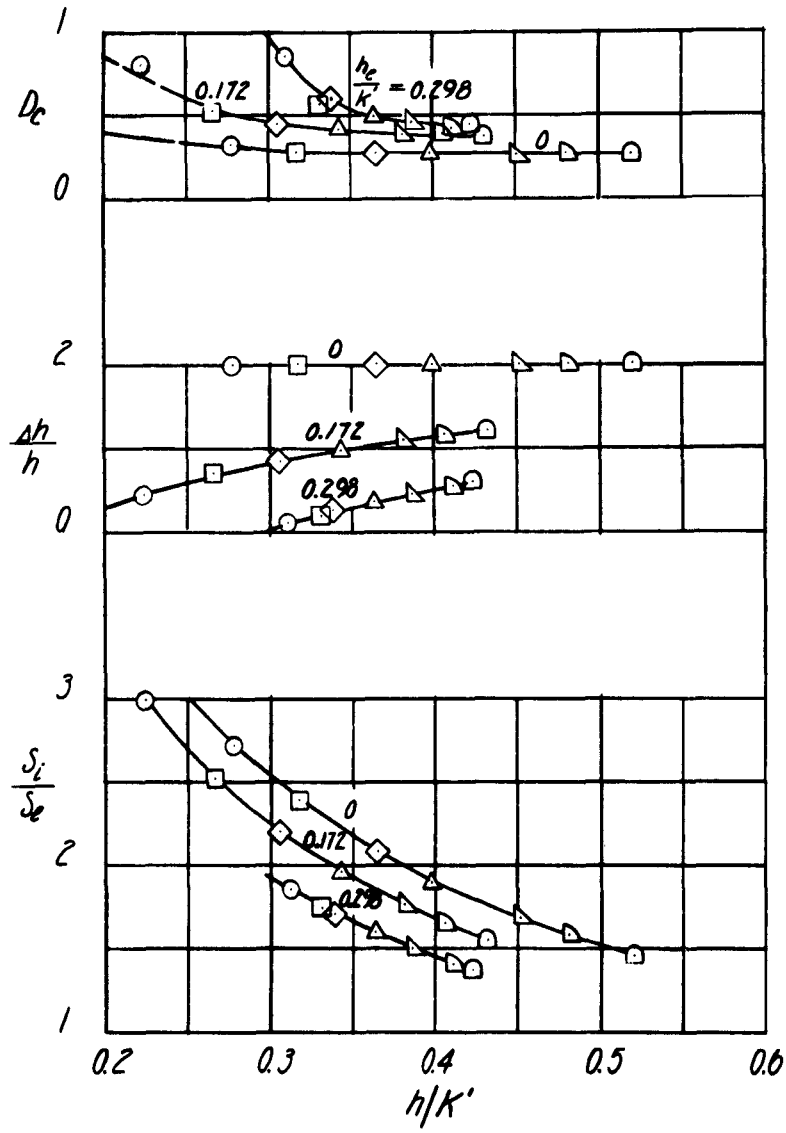

Figure 7 (Continued)

(e) $\frac{S}{S_1} = 16.957$

FIGURE 7e

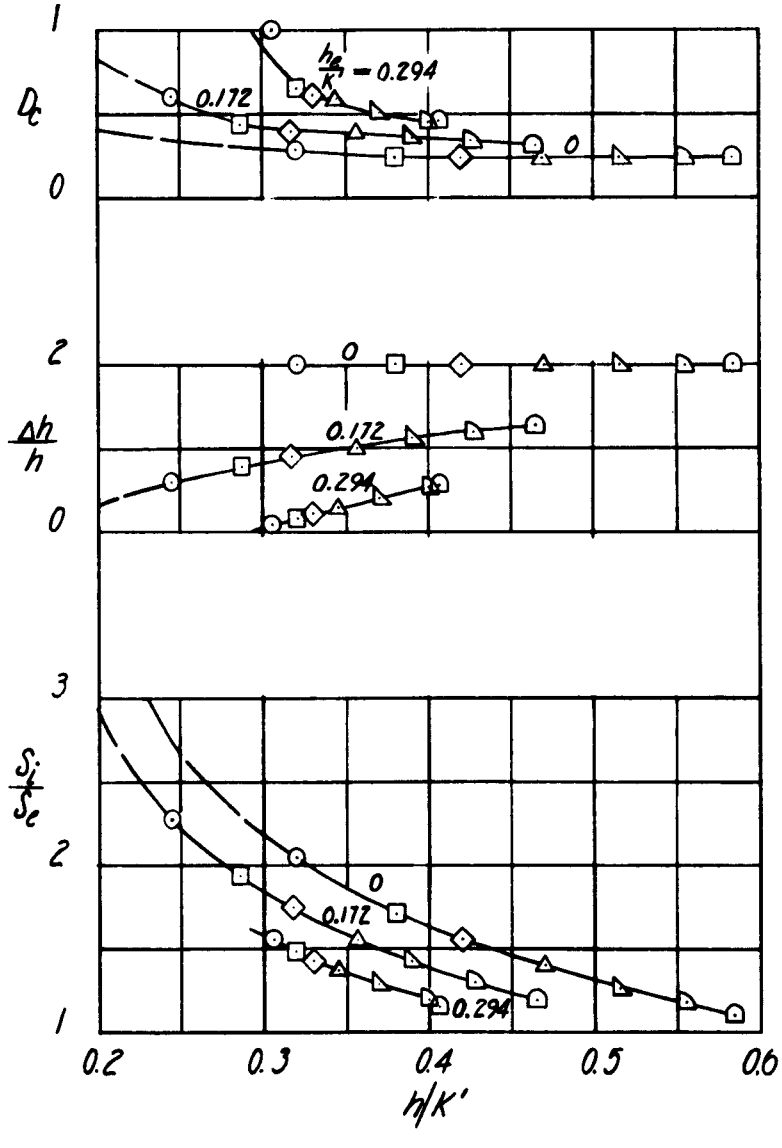

Figure 7 (Concluded)

(f) $\frac{S}{S_1} = 26.315$

FIGURE 7f

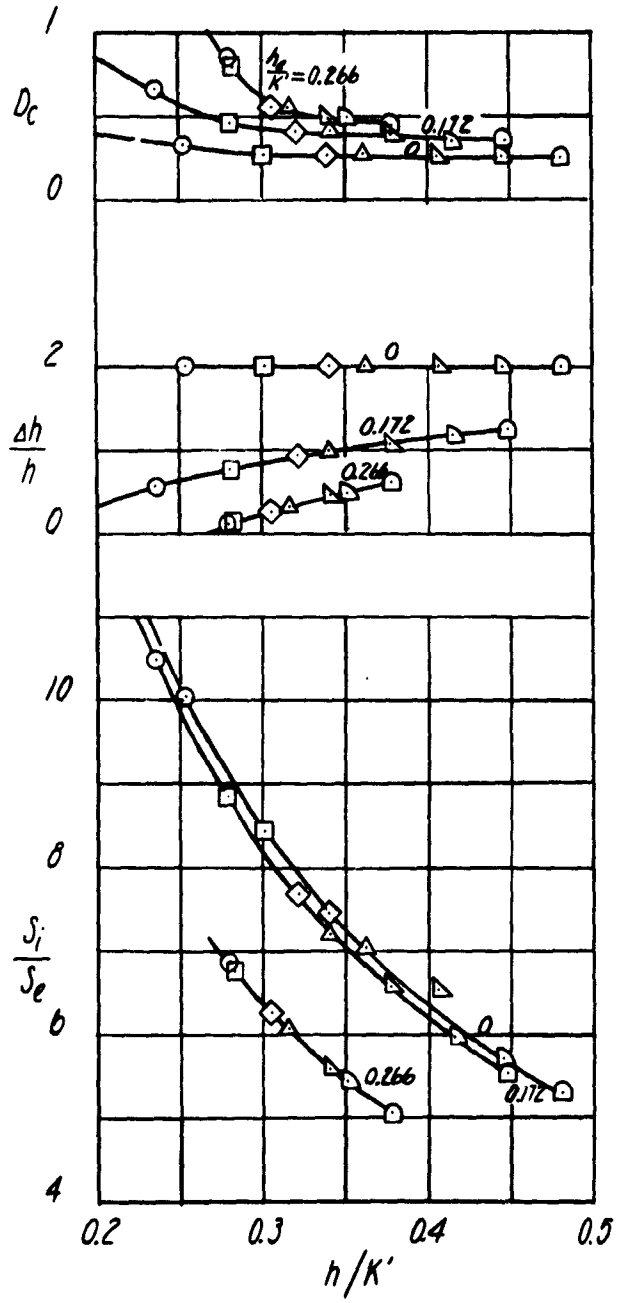

Figure 8 - Variation of the Parameters D_c, $\Delta h/h$, and S_i/S_e With h/k' for Several Values of h_e/k'. $\theta = 15^0$

(a) $\frac{S}{S_i} = 5.782$

FIGURE 8a

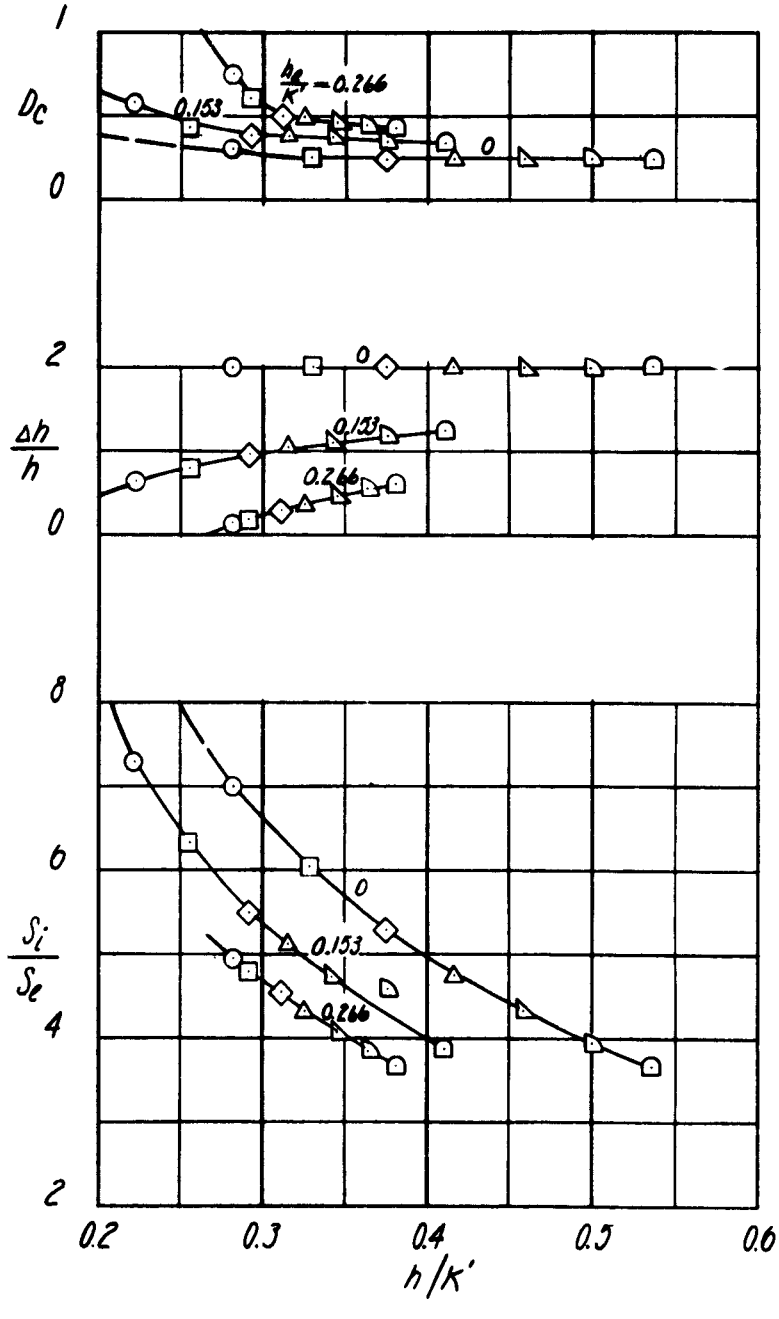

Figure 8 (Continued)
(b) $\frac{S}{S_1}$ = 7.868

FIGURE 8b

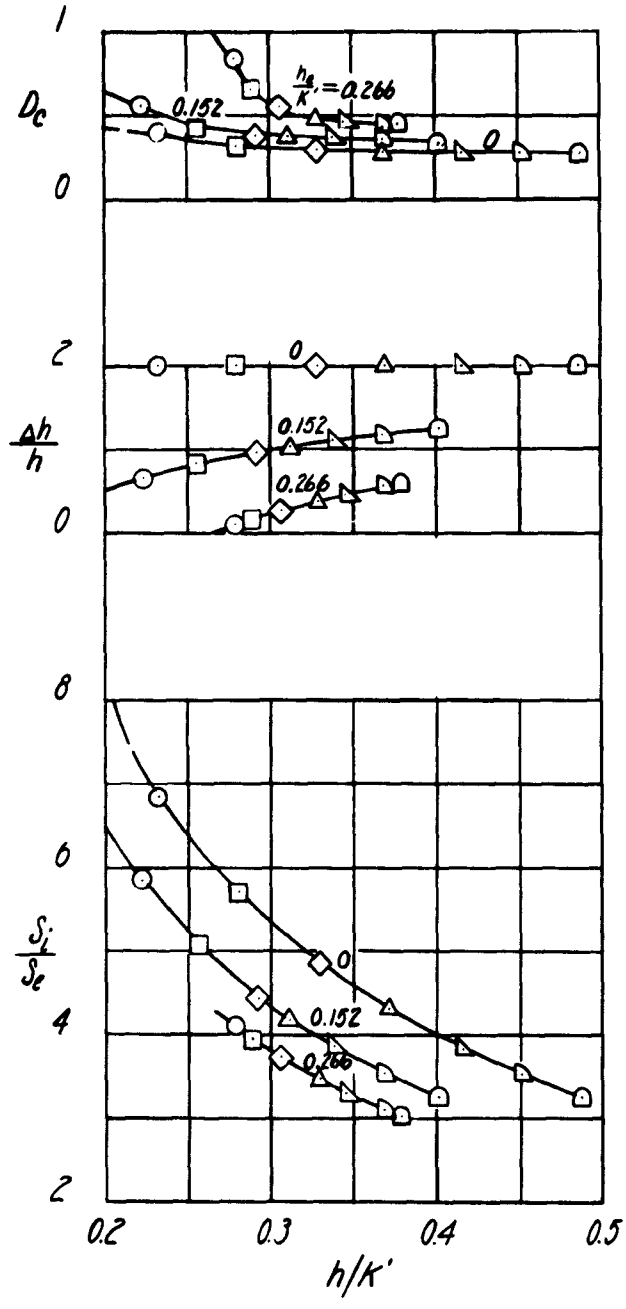

Figure 8 (Continued)

(c) $\frac{S}{S_i} = 9.666$

FIGURE 8c

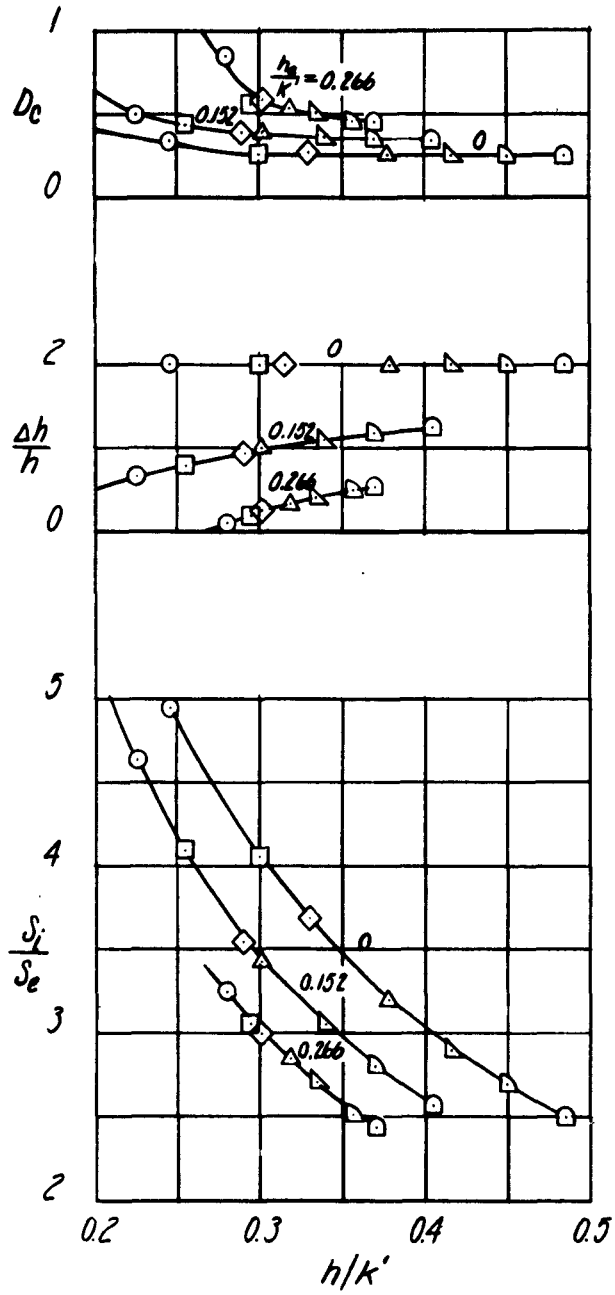

Figure 8 (Continued)
(d) $\frac{S}{S_i}$ = 12.187

FIGURE 8d

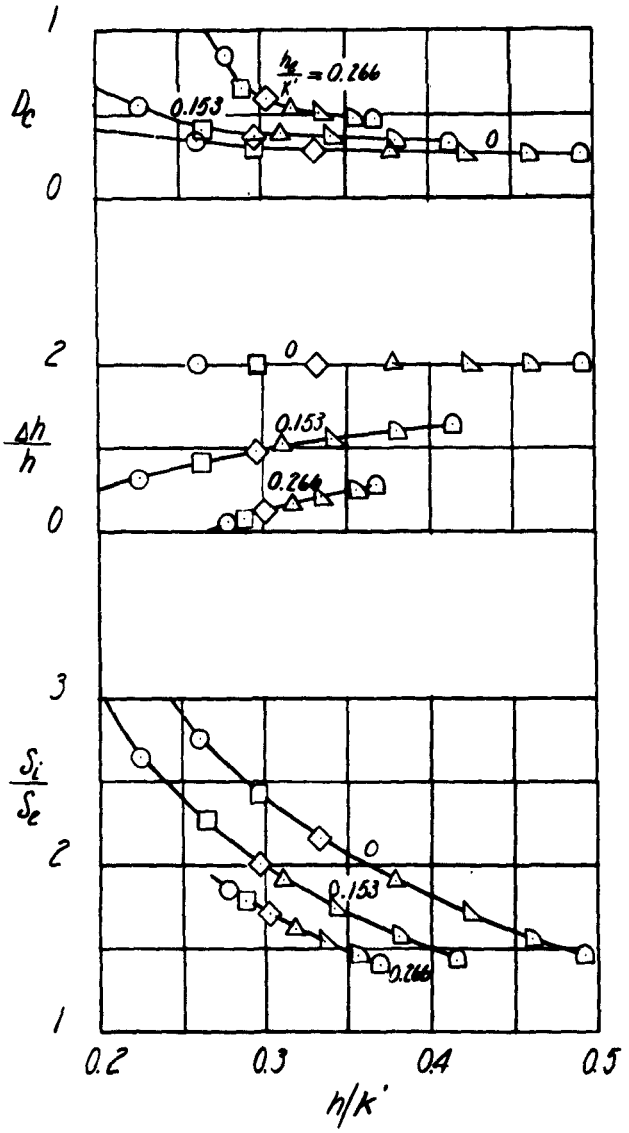

Figure 8 (Continued)
(e) $\frac{S}{S_i} = 16.619$

FIGURE 8e

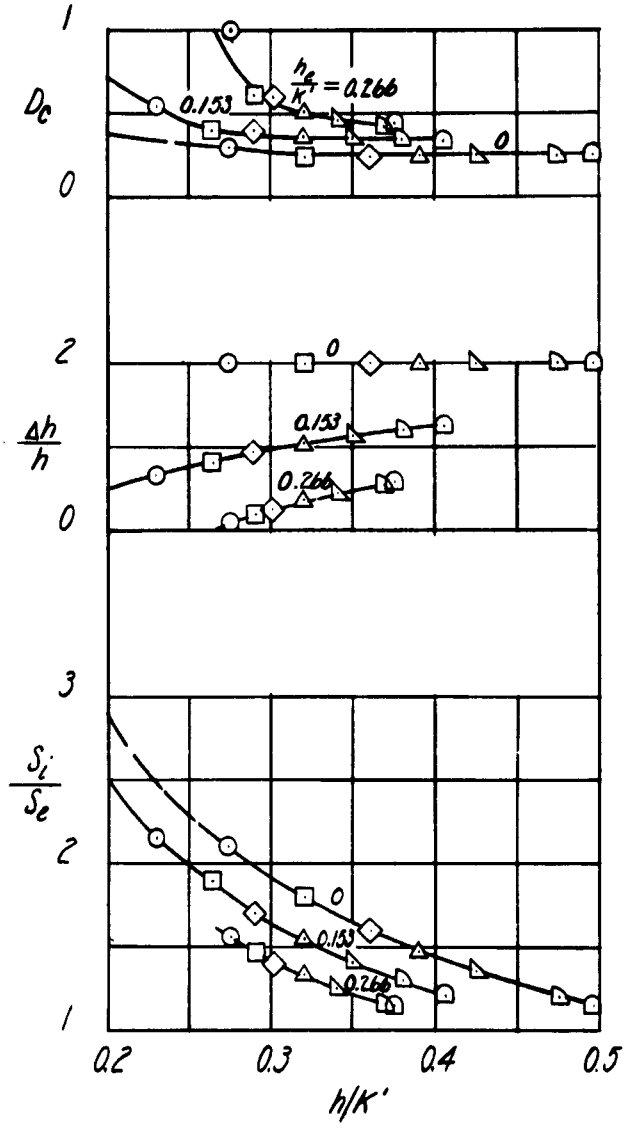

Figure 8 (Concluded)
(f) $\frac{S}{S_i}$ = 25.790

FIGURE 8f

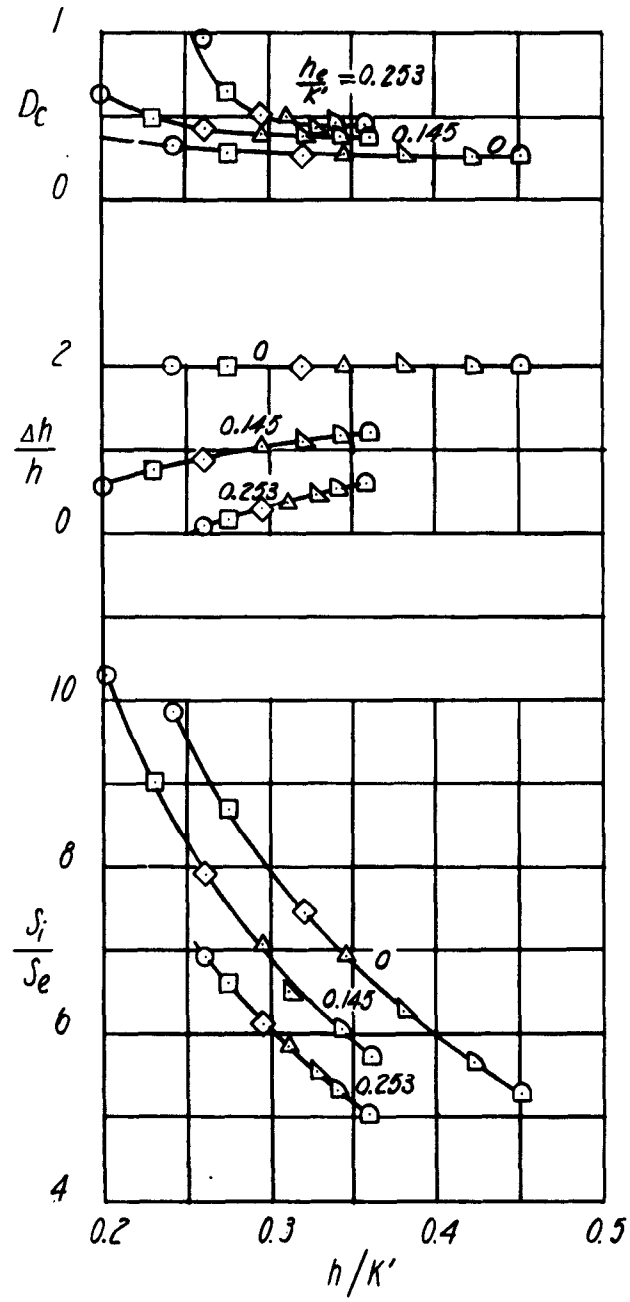

Figure 9 - Variation of the Parameters D_c, $\Delta h/h$, and S_i/S_e With h/k' for Several Values of h_e/k'. $\theta = 0^\circ$

(a) $\frac{S}{S_i} = 5.67$

FIGURE 9a

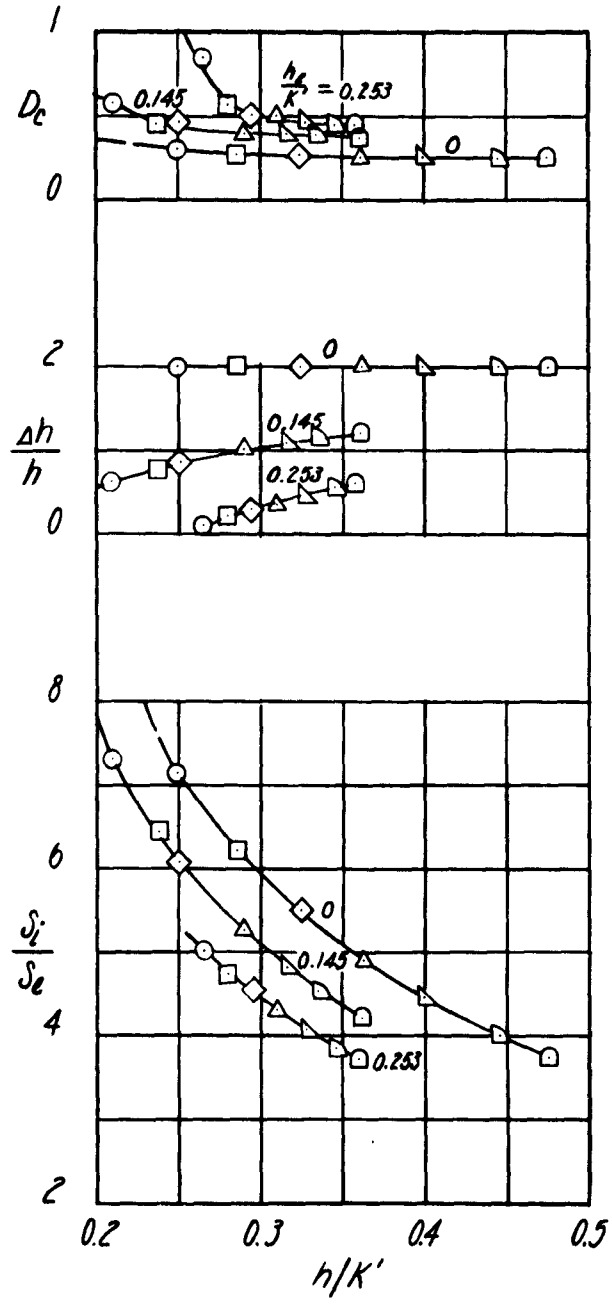

Figure 9 (Continued)
(b) $\frac{S}{S_1} = 7.72$

FIGURE 9b

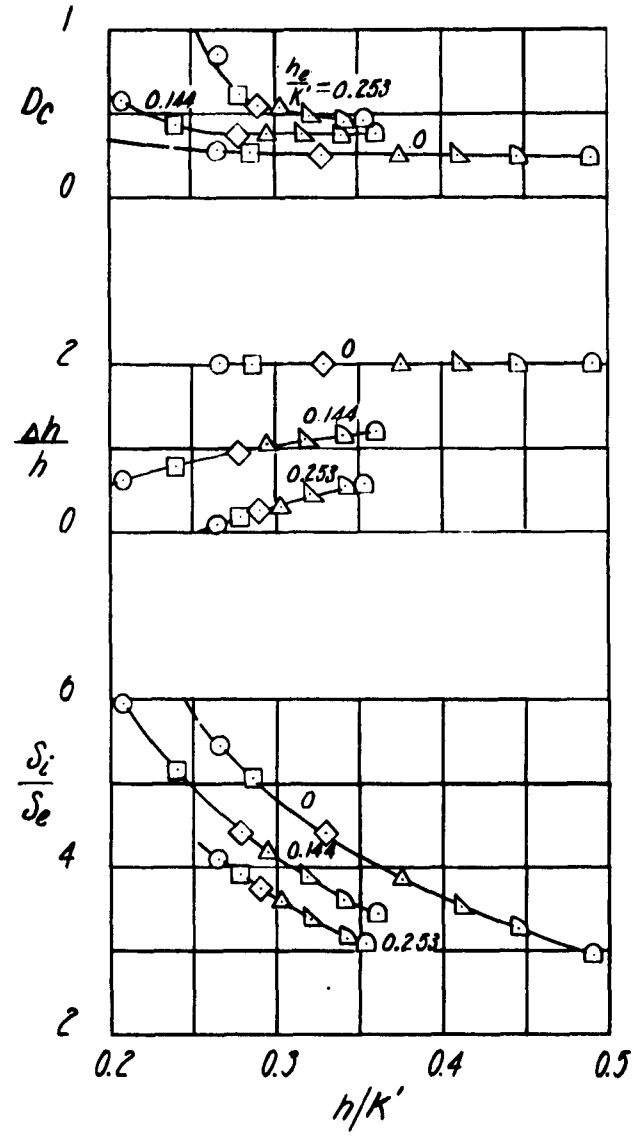

Figure 9 (Continued)
(c) $\frac{S}{S_1}$ = 9.48

FIGURE 9c

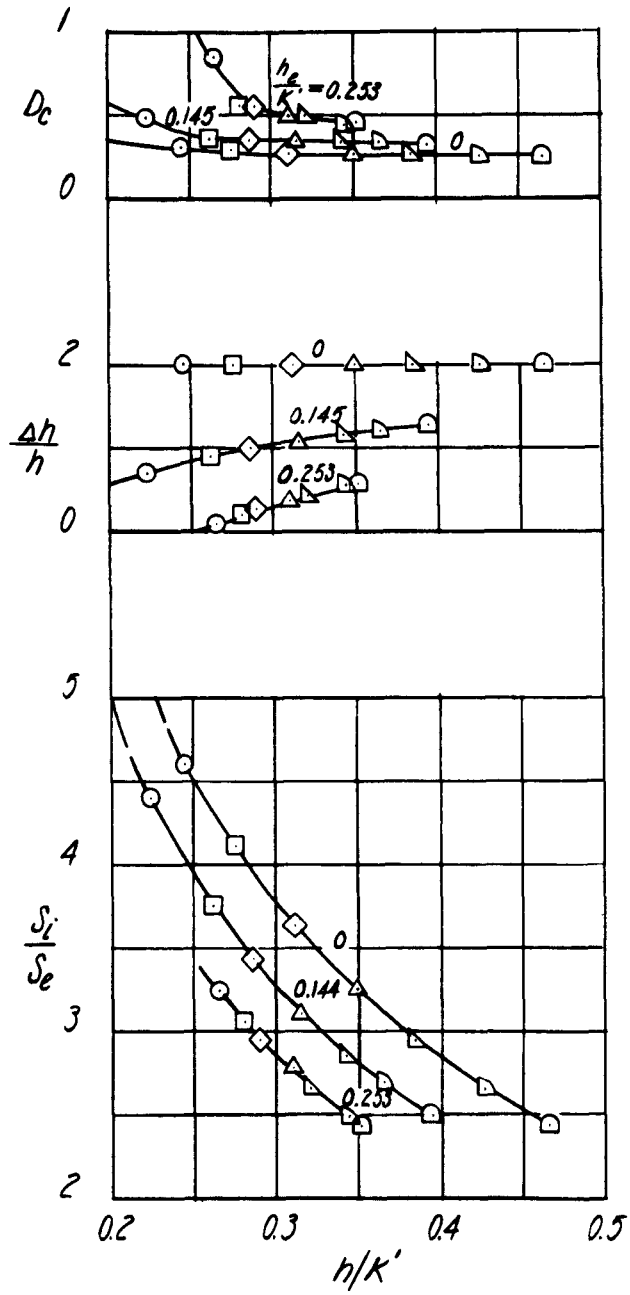

Figure 9 (Continued)

(d) $\frac{S}{S_i}$ = 11.96

FIGURE 9d

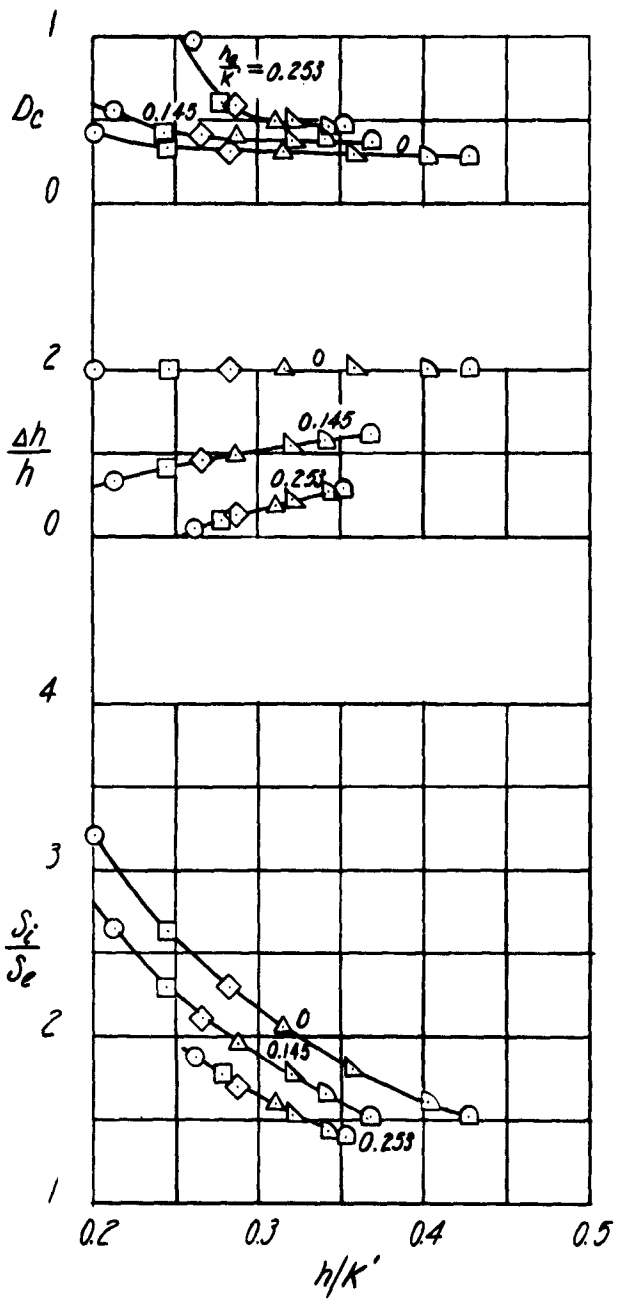

Figure 9 (Continued)
(e) $\frac{S}{S_i}$ = 16.31

FIGURE 9e

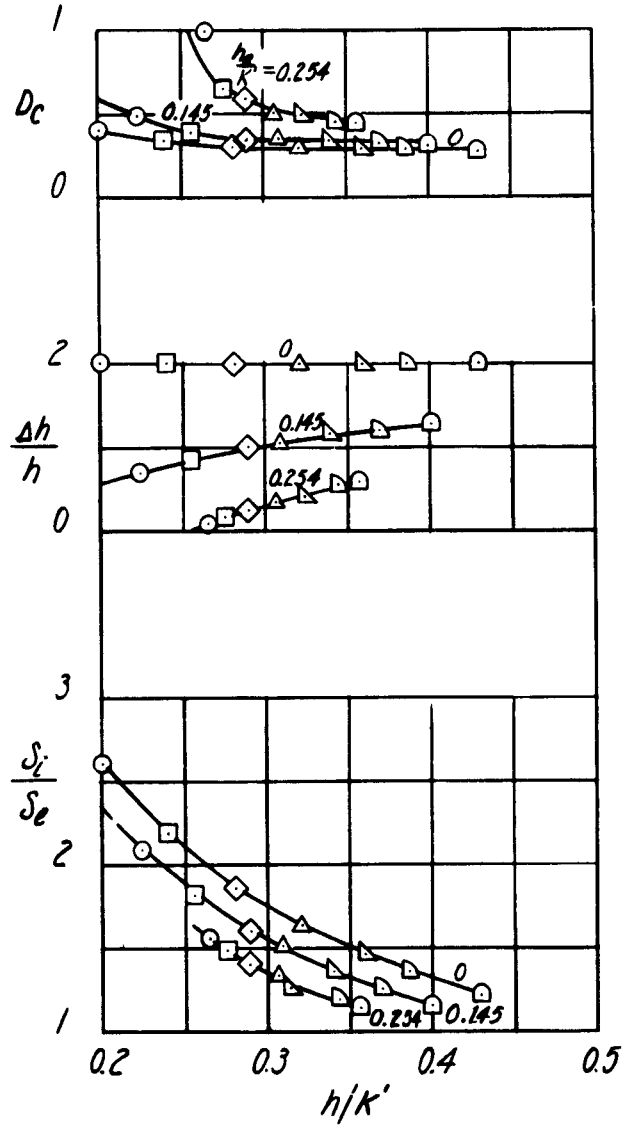

Figure 9 (Concluded)

(f) $\frac{S}{S_1}$ = 25.31

FIGURE 9f

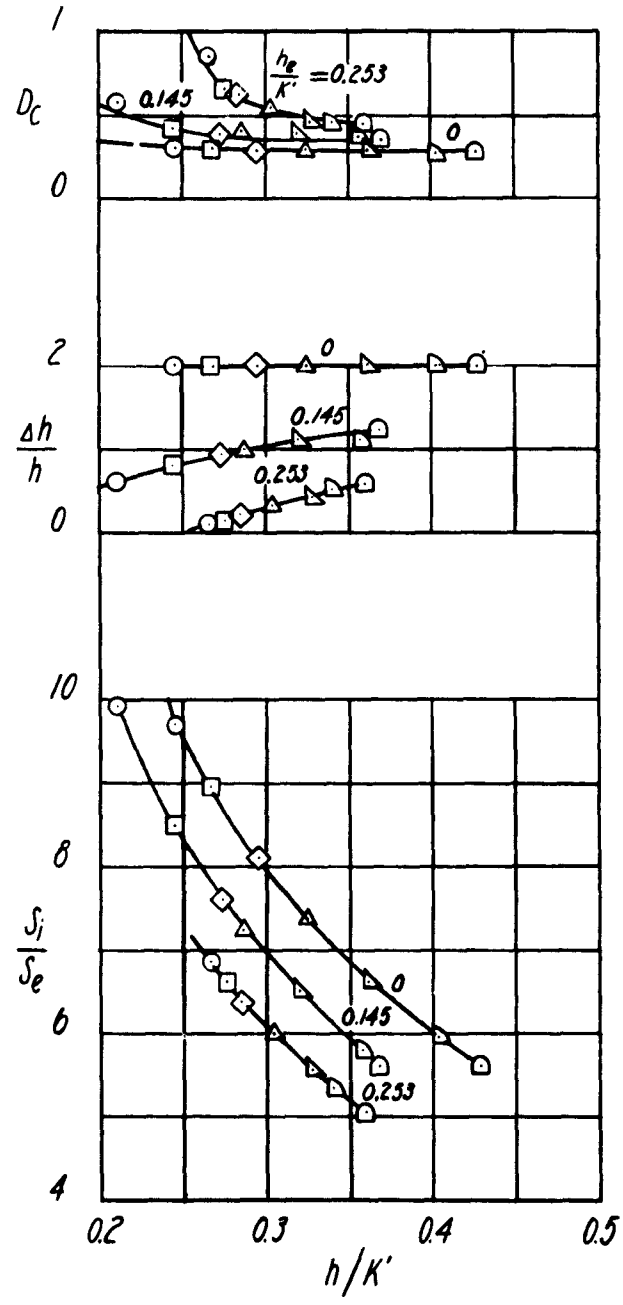

Figure 10 - Variation of the Parameters D_c, $\Delta h/h$, and S_i/S_e With h/k' for Several Values of h_e/k'. $\theta = -15°$

(a) $\frac{S}{S_i} = 5.57$

FIGURE 10a

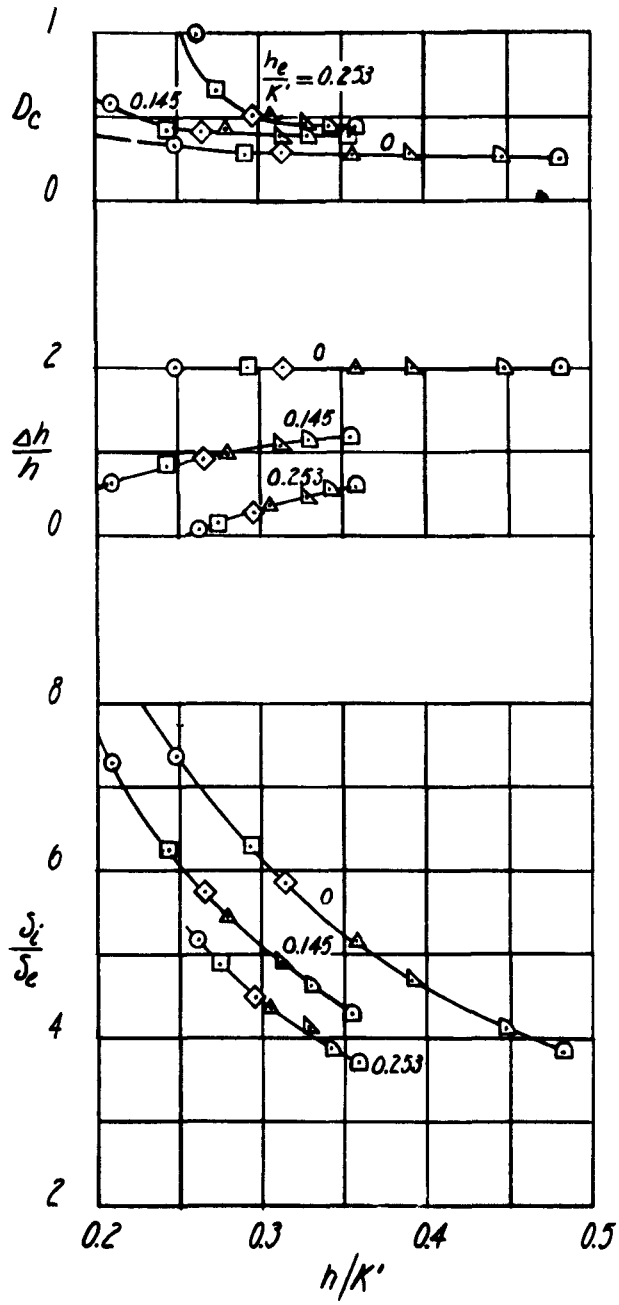

Figure 10 (Continued)
(b) $\frac{S}{S_1} = 7.57$

FIGURE 10b

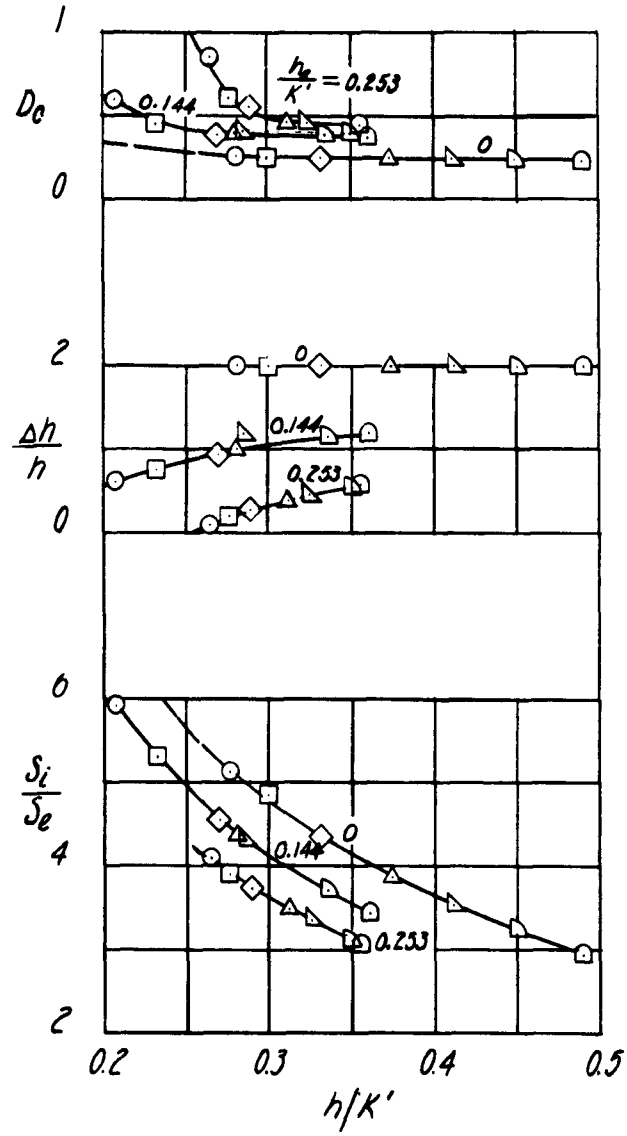

Figure 10 (Continued)
(c) $\frac{S}{S_1}$ = 9.30

FIGURE 10c

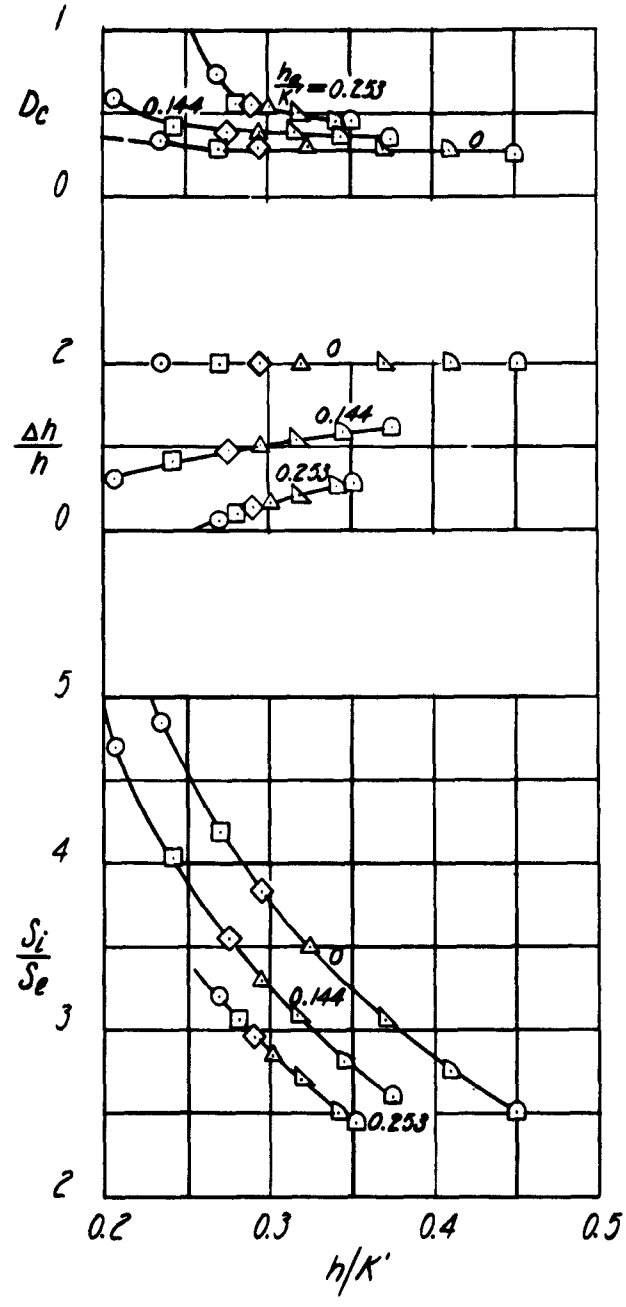

Figure 10 (Continued)
(d) $\frac{S}{S_1}$ = 11.73

FIGURE 10d

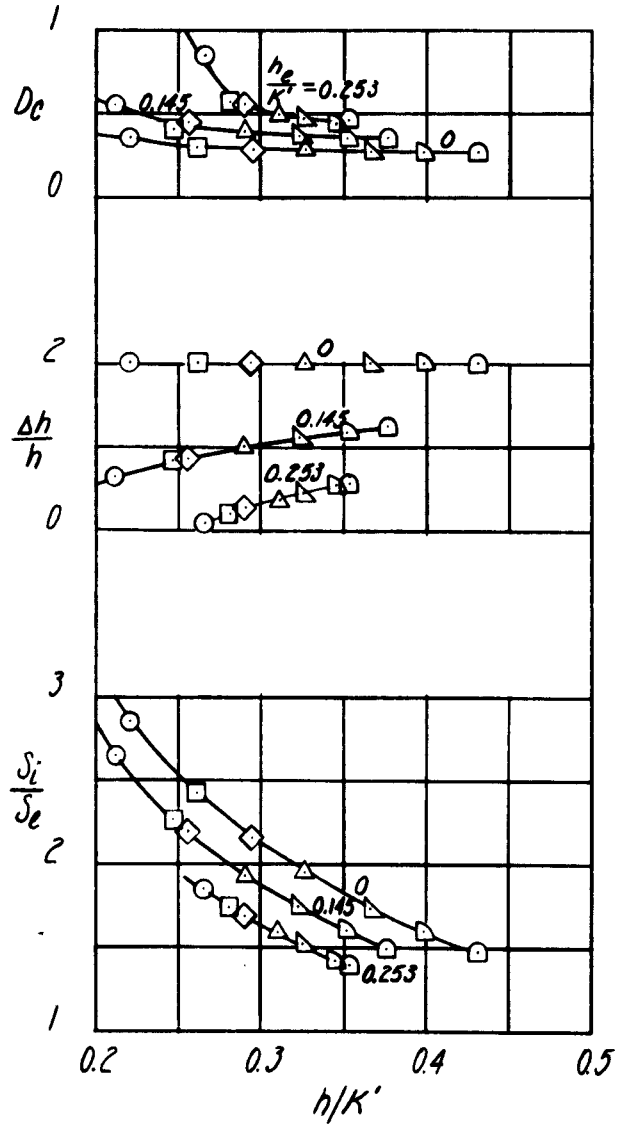

Figure 10 (Continued)
(e) $\frac{S}{S_1}$ = 16.00

FIGURE 10e

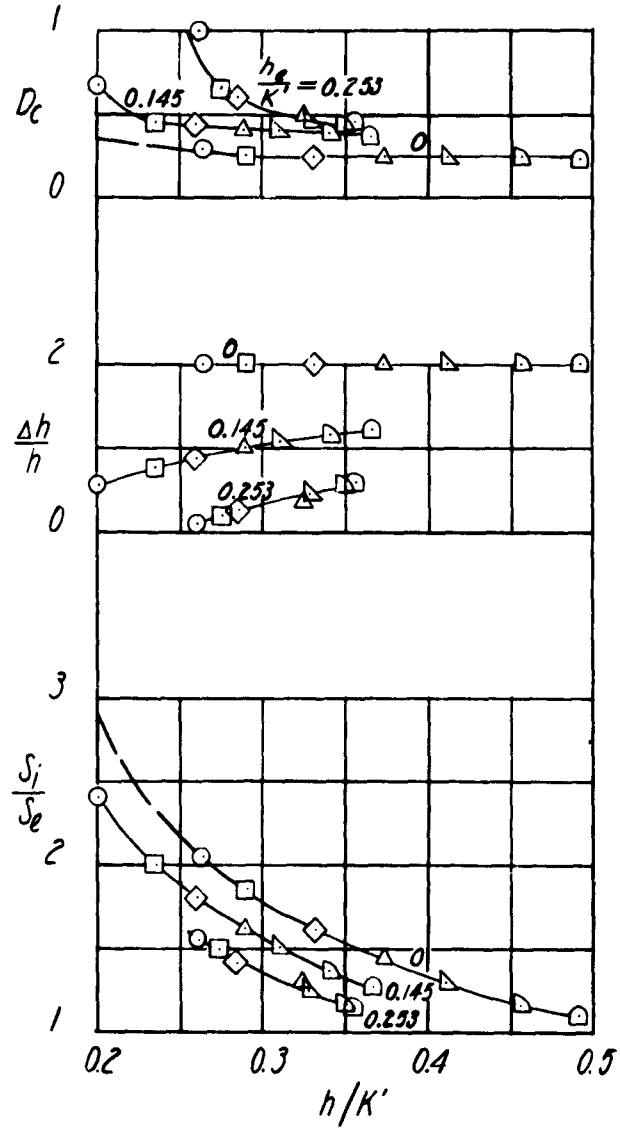

Figure 10 (Concluded)

(f) $\frac{S}{S_i} = 24.82$

FIGURE 10f

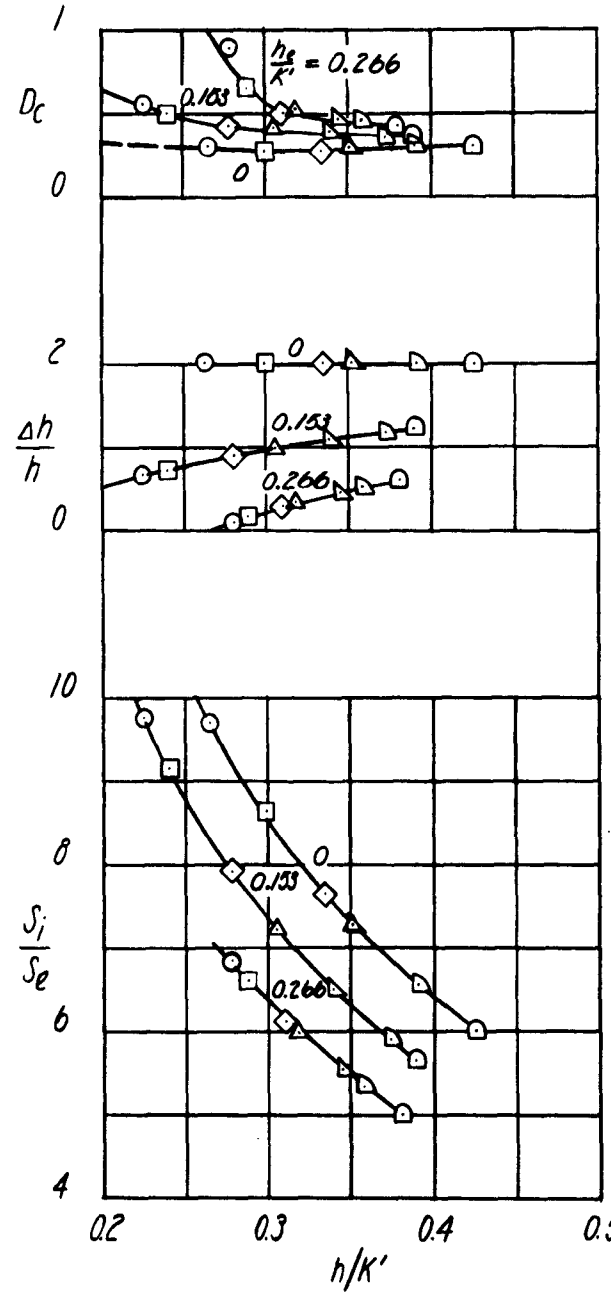

Figure 11 - Variation of the Parameters D_c, $\Delta h/h$, and S_i/S_e With h/k' for Several Values of h_e/k'. $\theta = -30^\circ$

(a) $\frac{S}{S_i} = 5.46$

FIGURE 11a

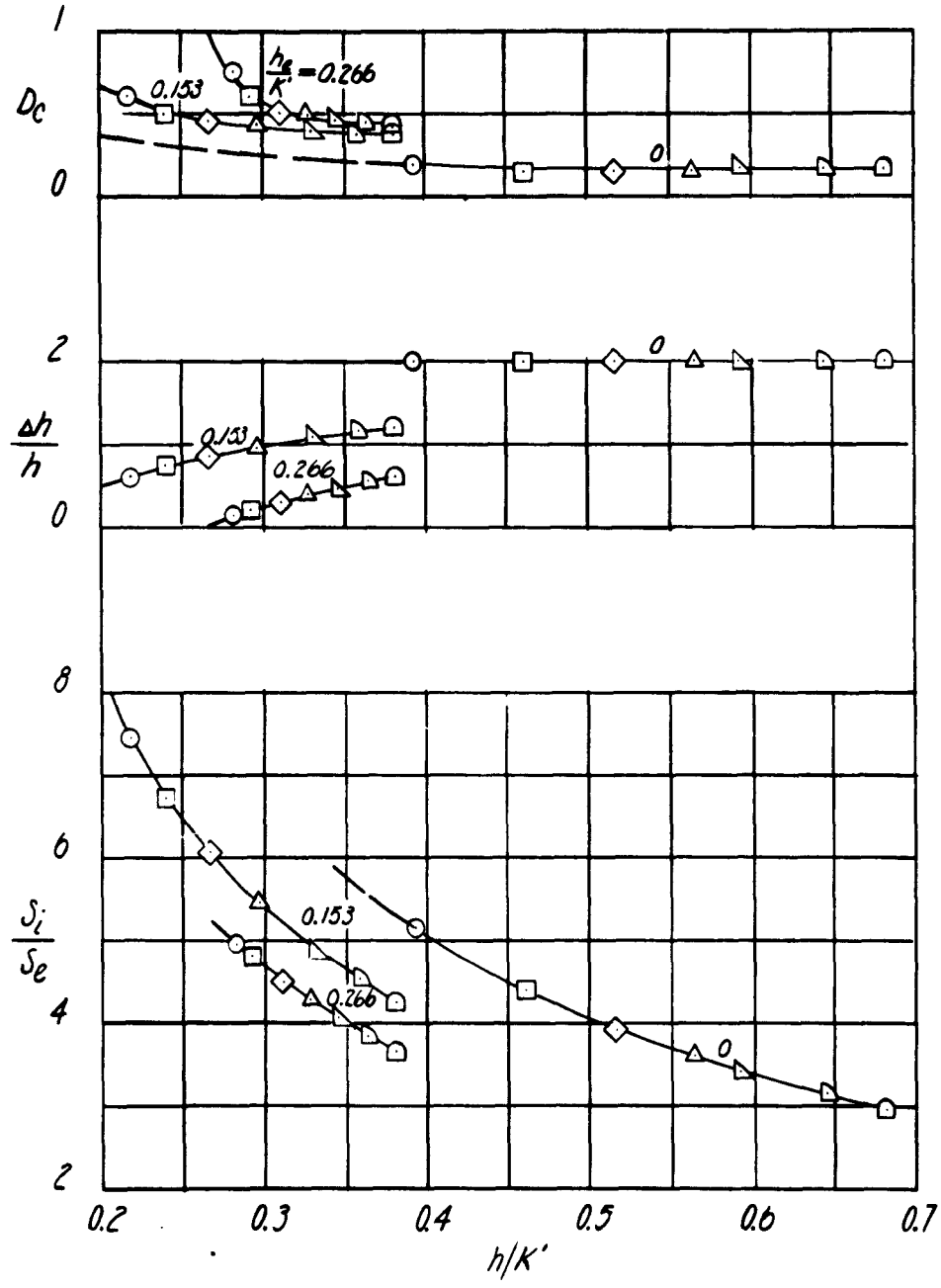

Figure 11 (Continued)
(b) $\frac{S}{S_i}$ = 7.44

FIGURE 11b

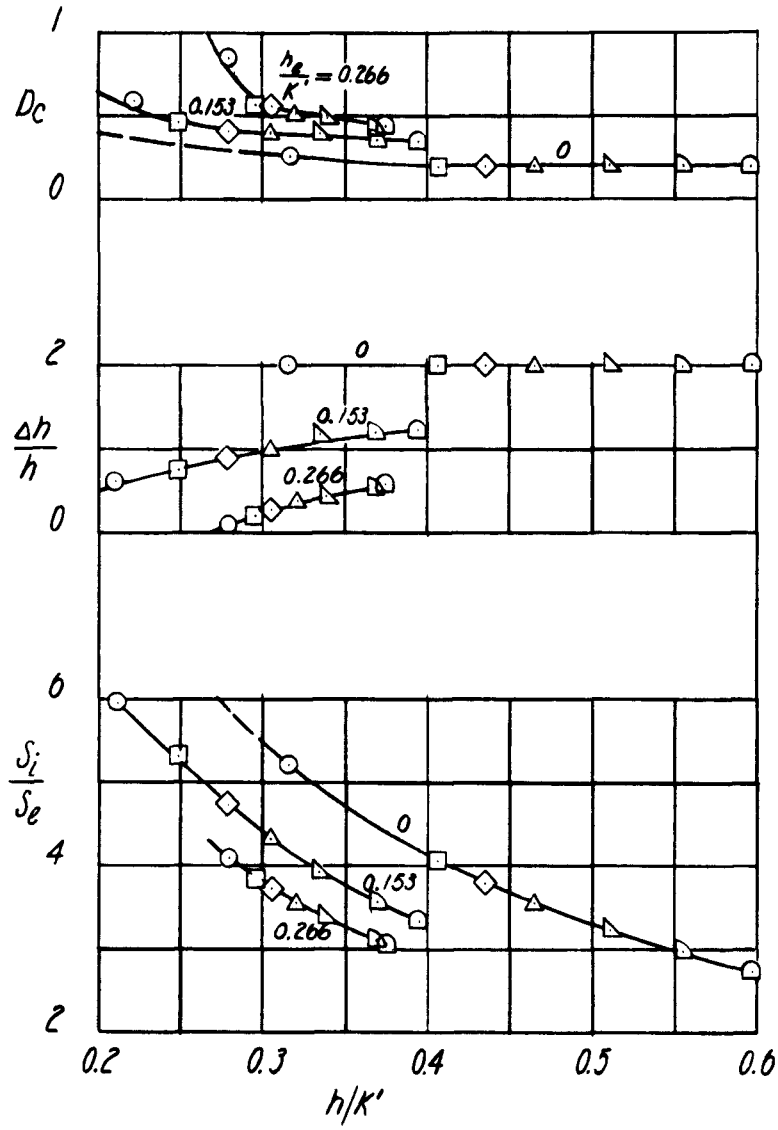

Figure 11 (Continued)
(c) $\frac{S}{S_i} = 9.14$

FIGURE 11c

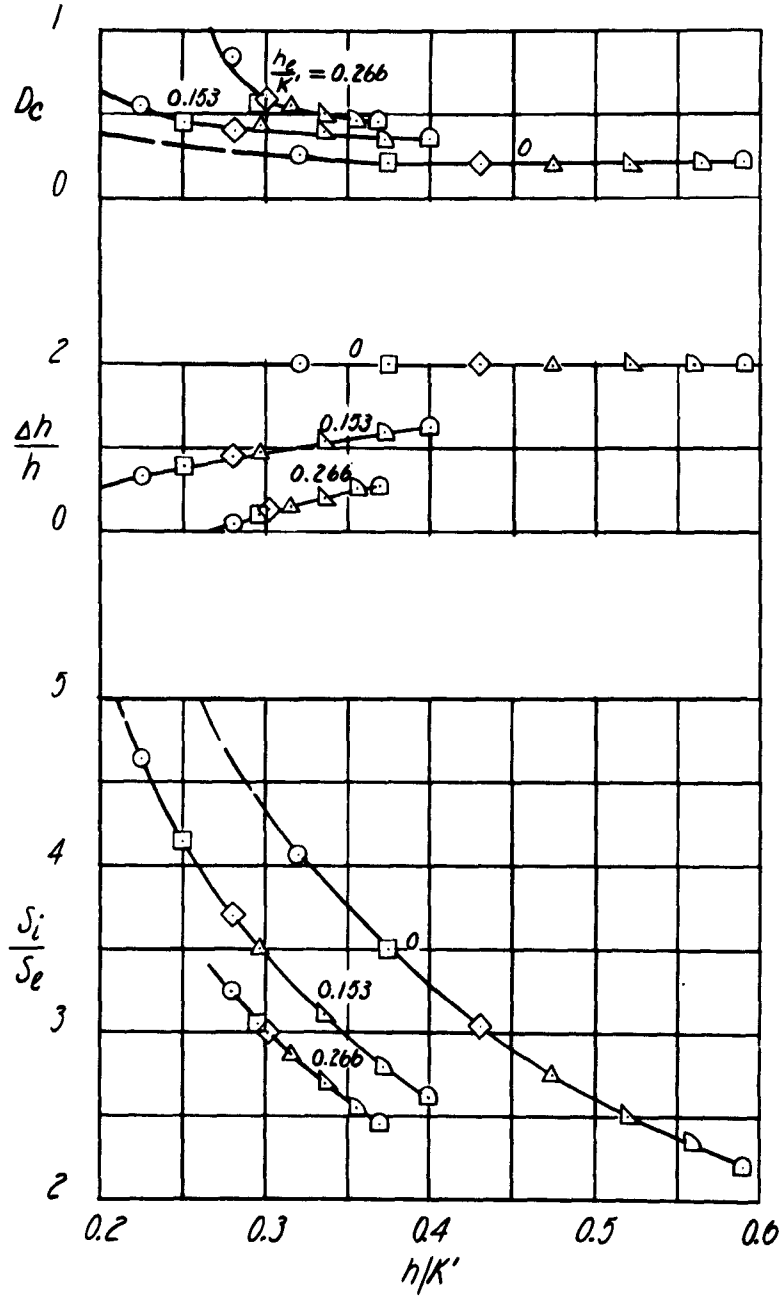

Figure 11 (Continued)

(d) $\frac{S}{S_i} = 11.52$

FIGURE 11d

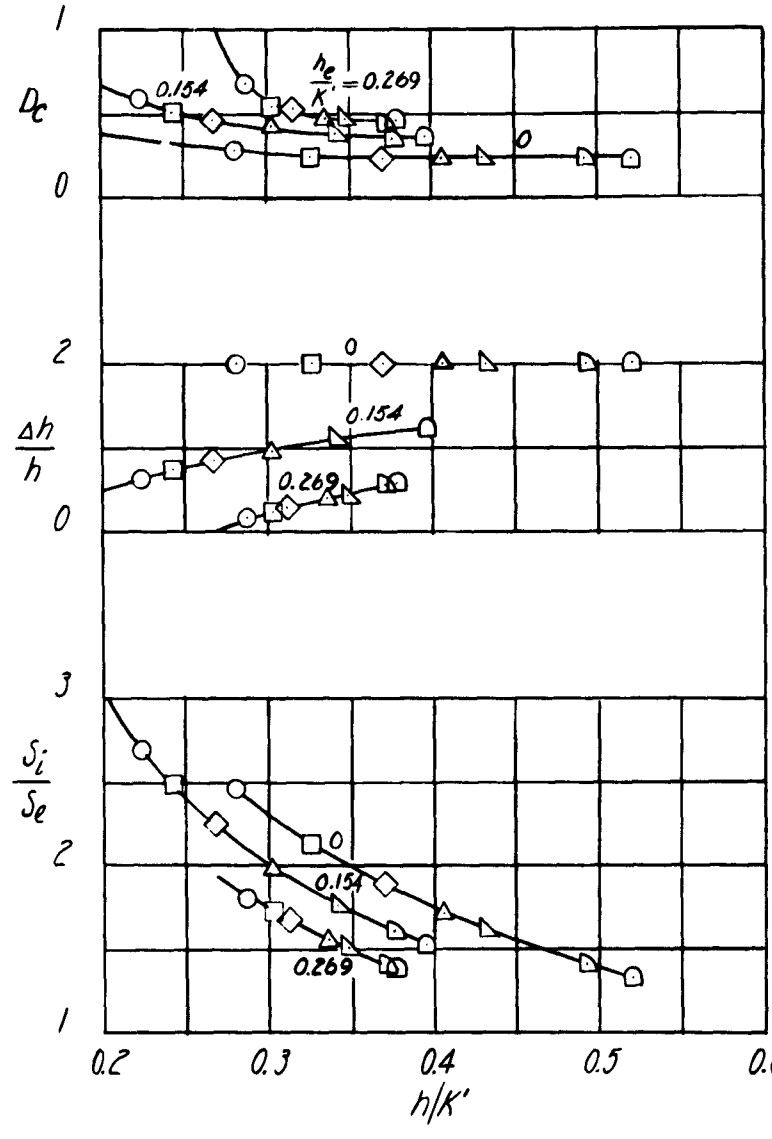

Figure 11 (Continued)
(e) $\frac{S}{S_i}$ = 15.71

FIGURE 11e

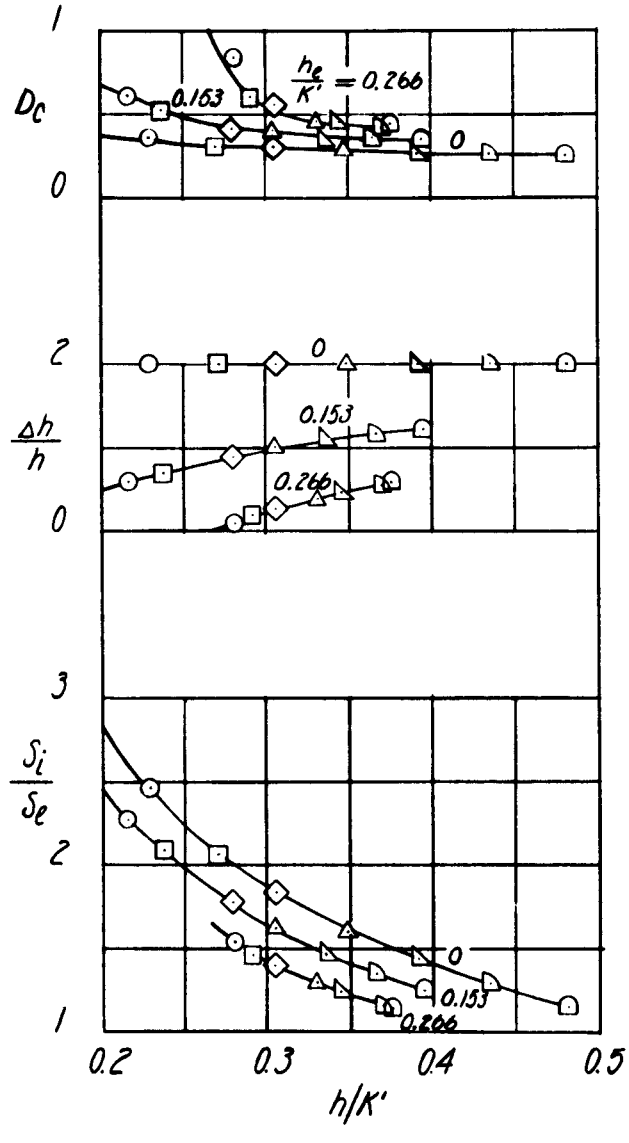

Figure 11 (Concluded)
(f) $\frac{S}{S_1}$ = 24.37

FIGURE 11f

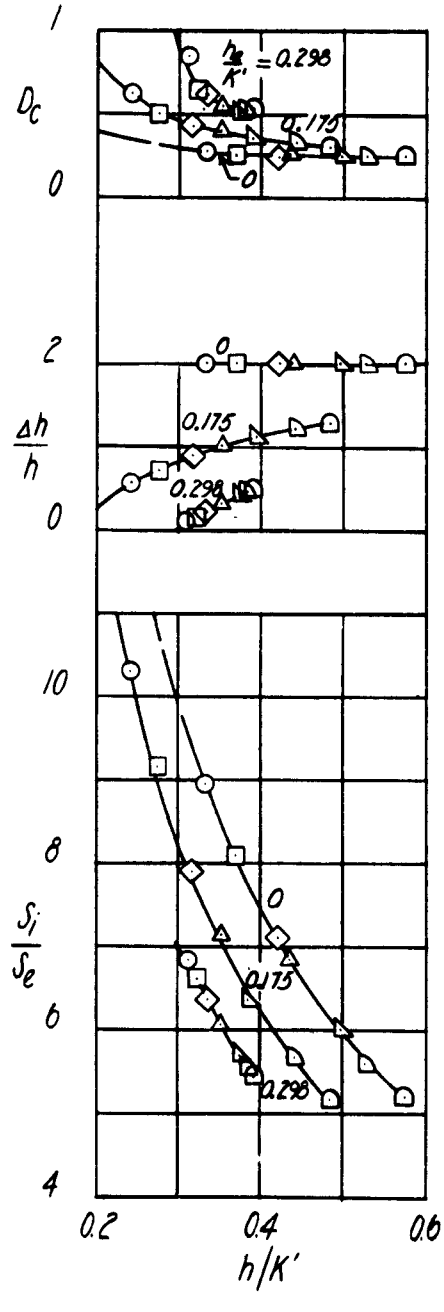

Figure 12 - Variation of the Parameters D_c, $\Delta h/h$, and S_i/S_e With h/k' for Several Values of h_e/k'. $\theta = -45°$

(a) $\frac{S}{S_i} = 5.38$

FIGURE 12a

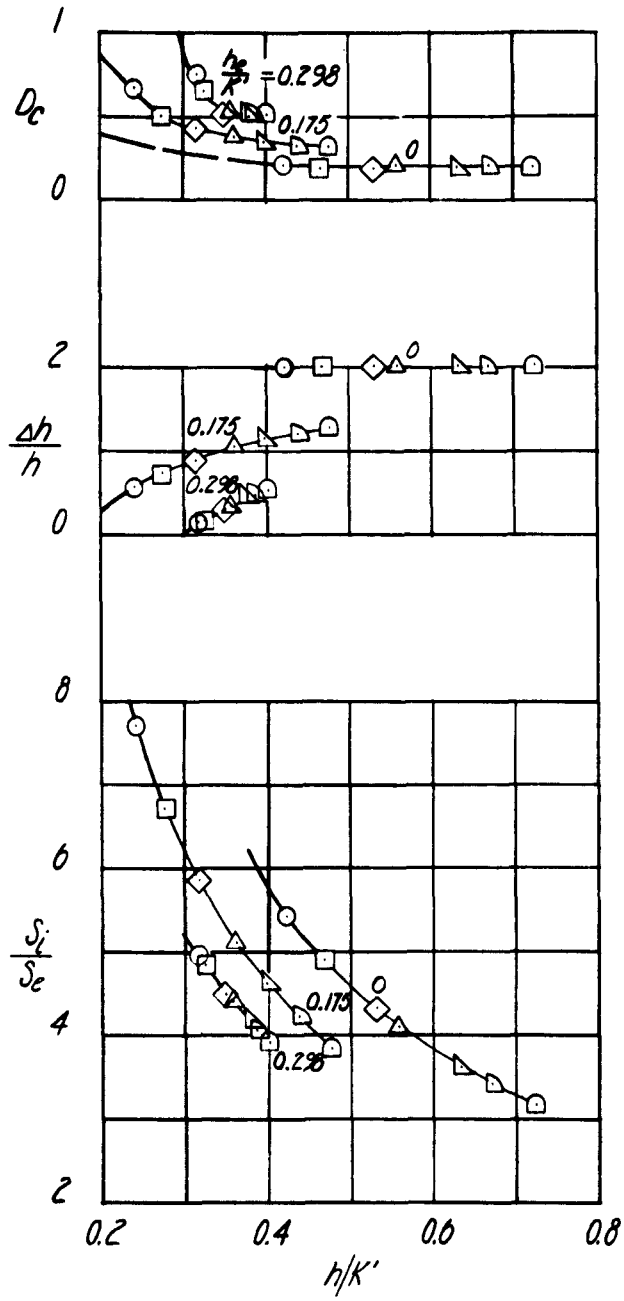

Figure 12 (Continued)

(b) $\frac{S}{S_i}$ = 7.32

FIGURE 12b

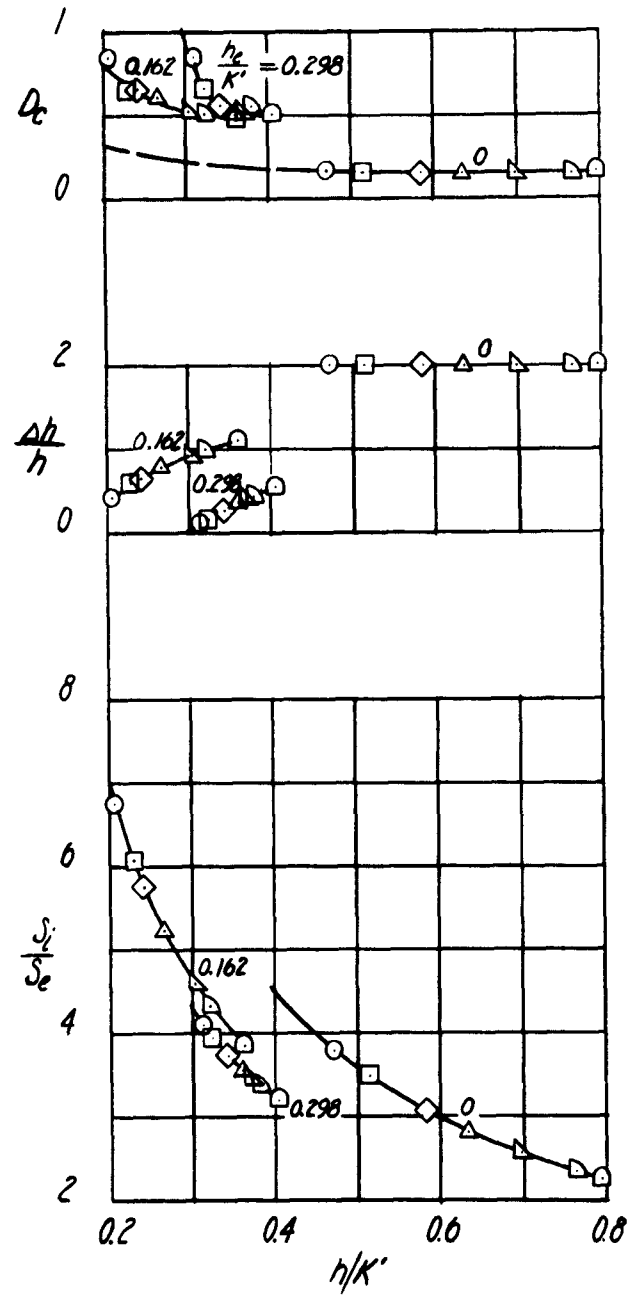

Figure 12 (Continued)
(c) $\frac{S}{S_i}$ = 8.99

FIGURE 12c

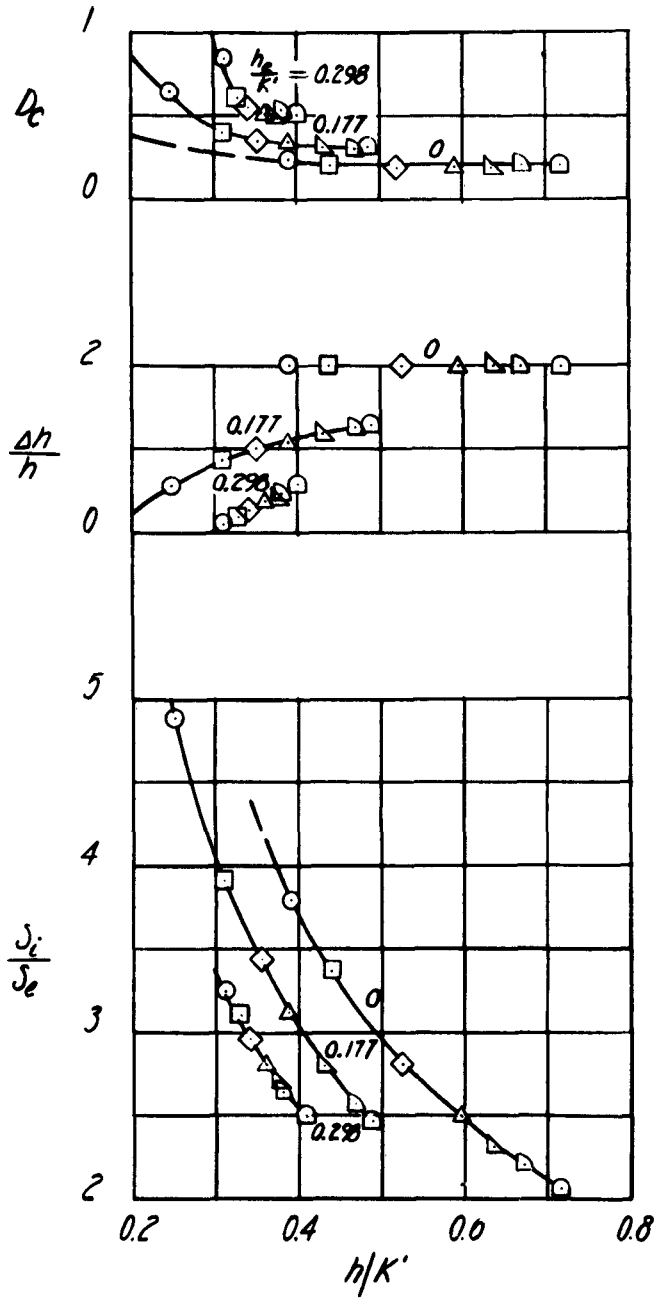

Figure 12 (Continued)
(d) $\frac{S}{S_1} = 11.34$

FIGURE 12d

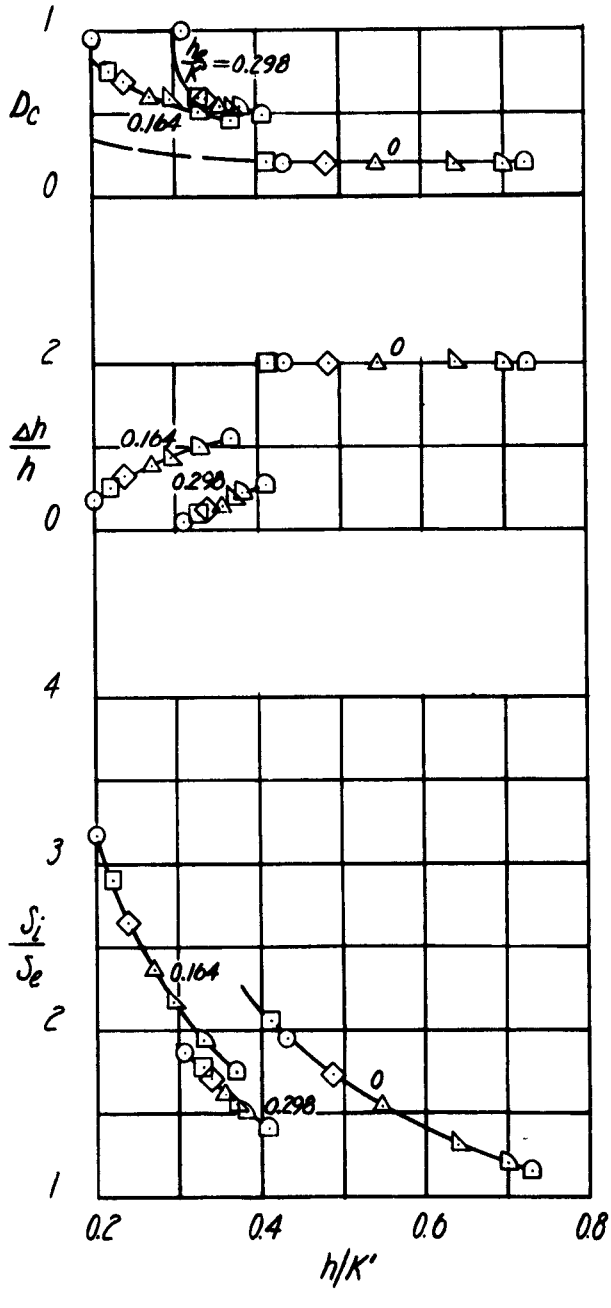

Figure 12 (Continued)
(e) $\frac{S}{S_1}$ = 15.46

FIGURE 12e

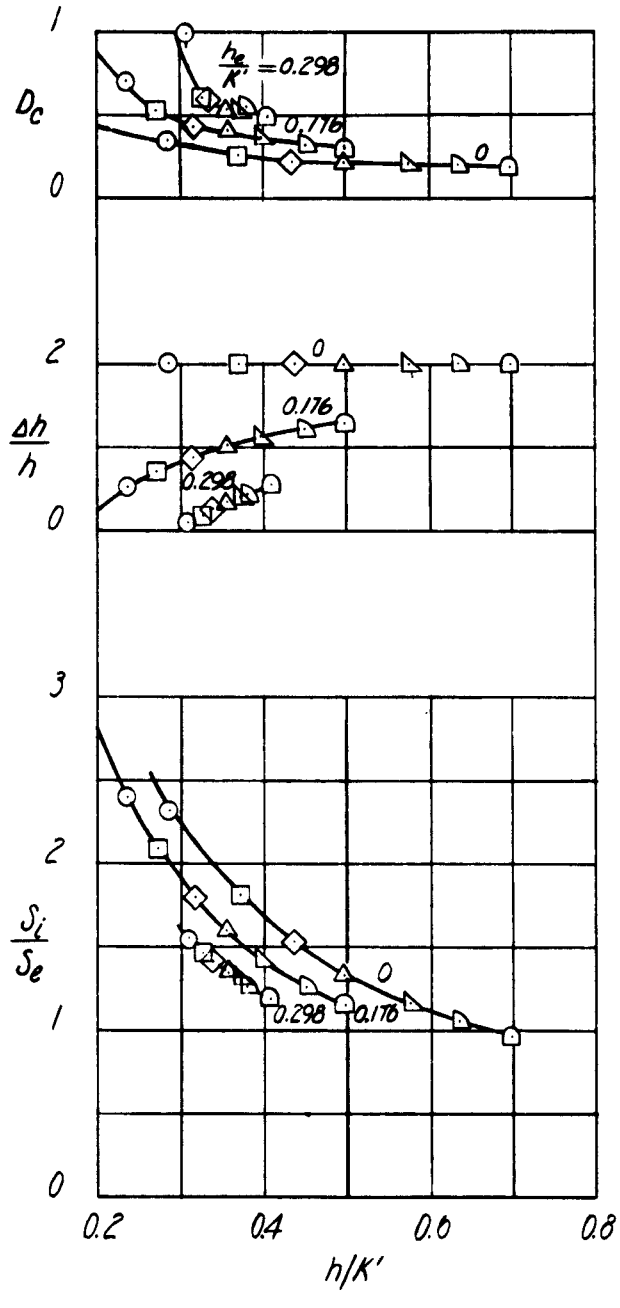

Figure 12 (Concluded)

(f) $\frac{S}{S_1}$ = 23.99

FIGURE 12f

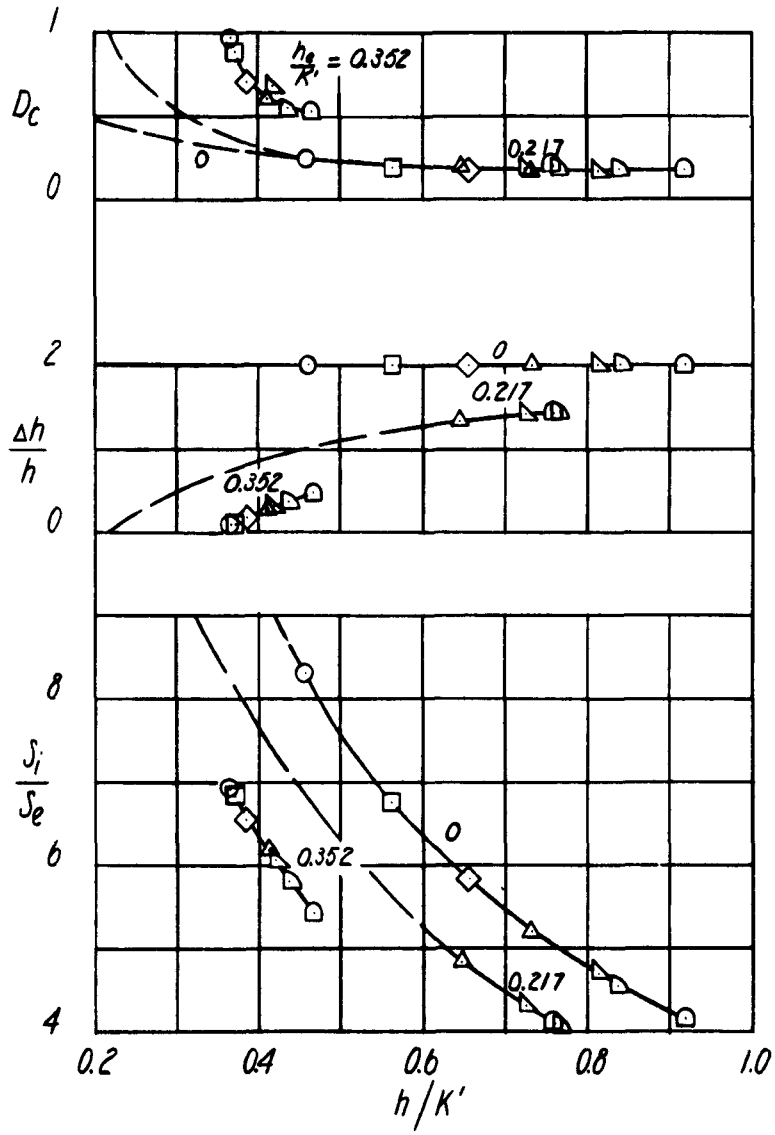

Figure 13 - Variation of the Parameters D_c, $\Delta h/h$, and S_i/S_e With h/k' for Several Values of h_e/k'. $\theta = -60^\circ$

(a) $\frac{S}{S_i} = 5.31$

FIGURE 13a

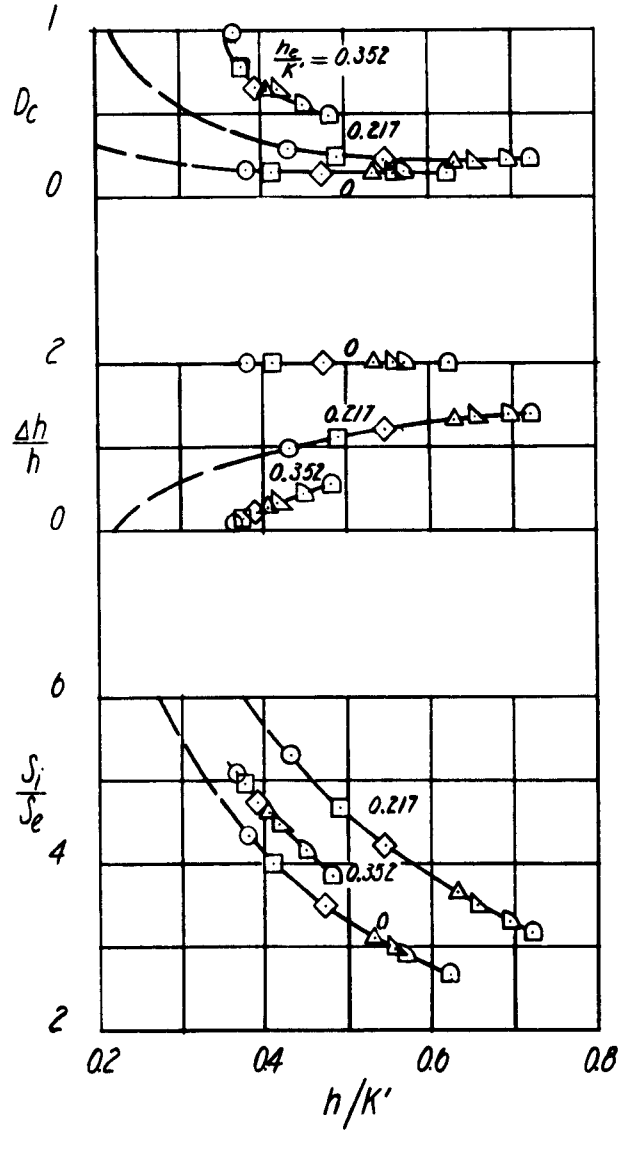

Figure 13 (Continued)
(b) $\frac{S}{S_i} = 7.23$

FIGURE 13b

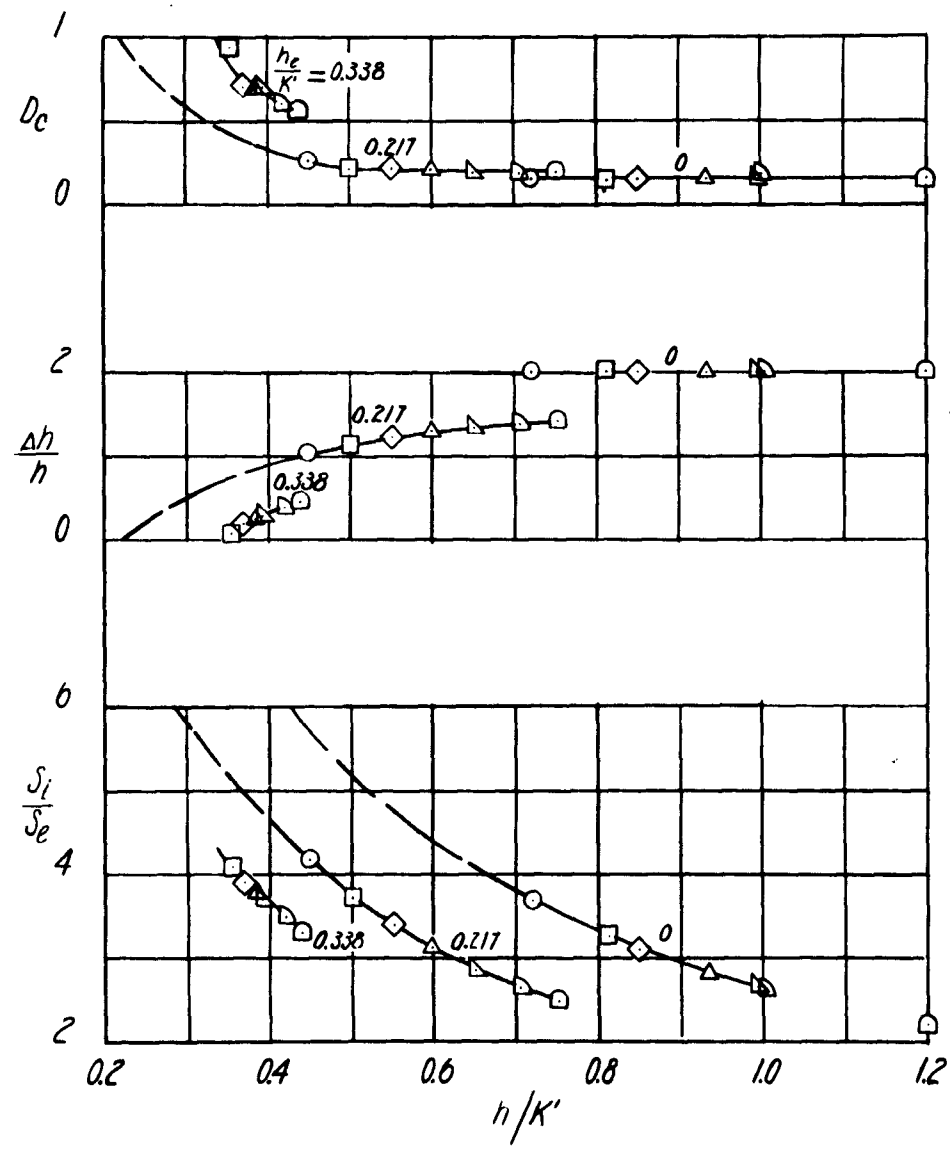

Figure 13 (Continued)
(c) $\frac{S}{S_1}$ = 8.88

FIGURE 13c

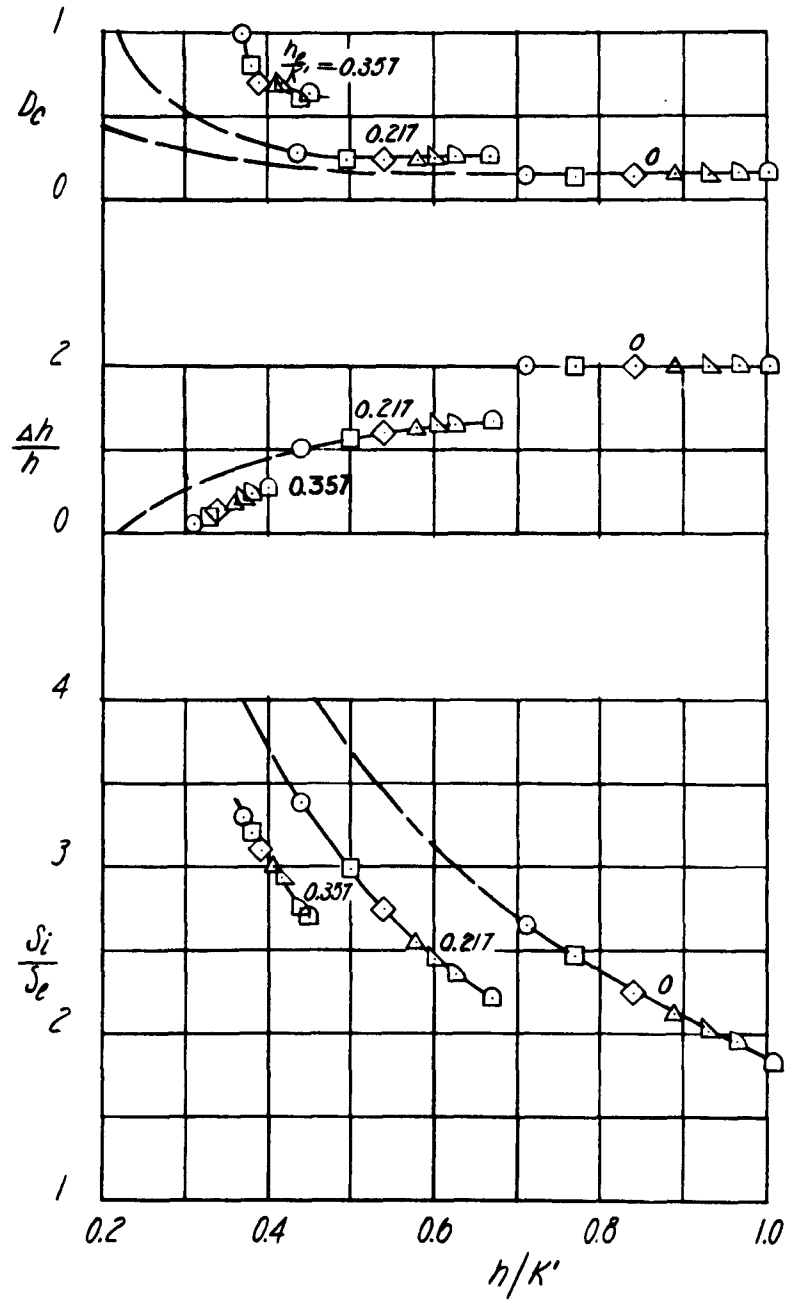

Figure 13 (Continued)

(d) $\frac{S}{S_i} = 11.20$

FIGURE 13d

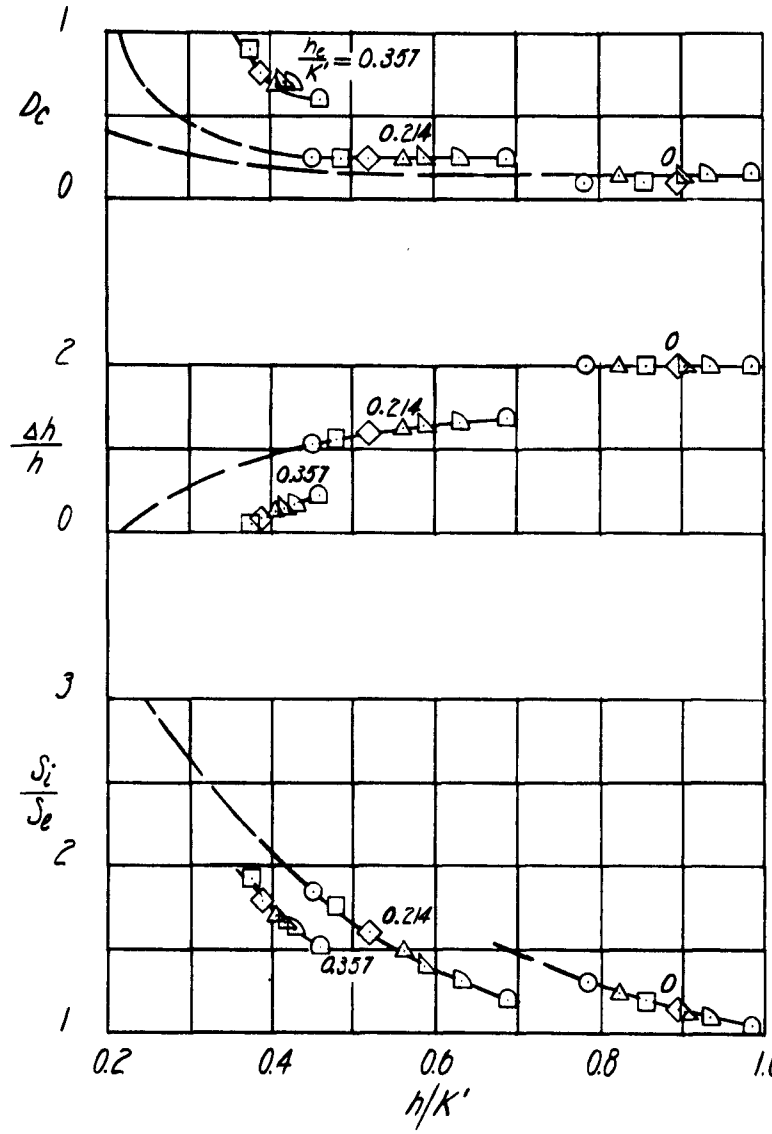

Figure 13 (Continued)

(e) $\frac{S}{S_i} = 15.27$

FIGURE 13e

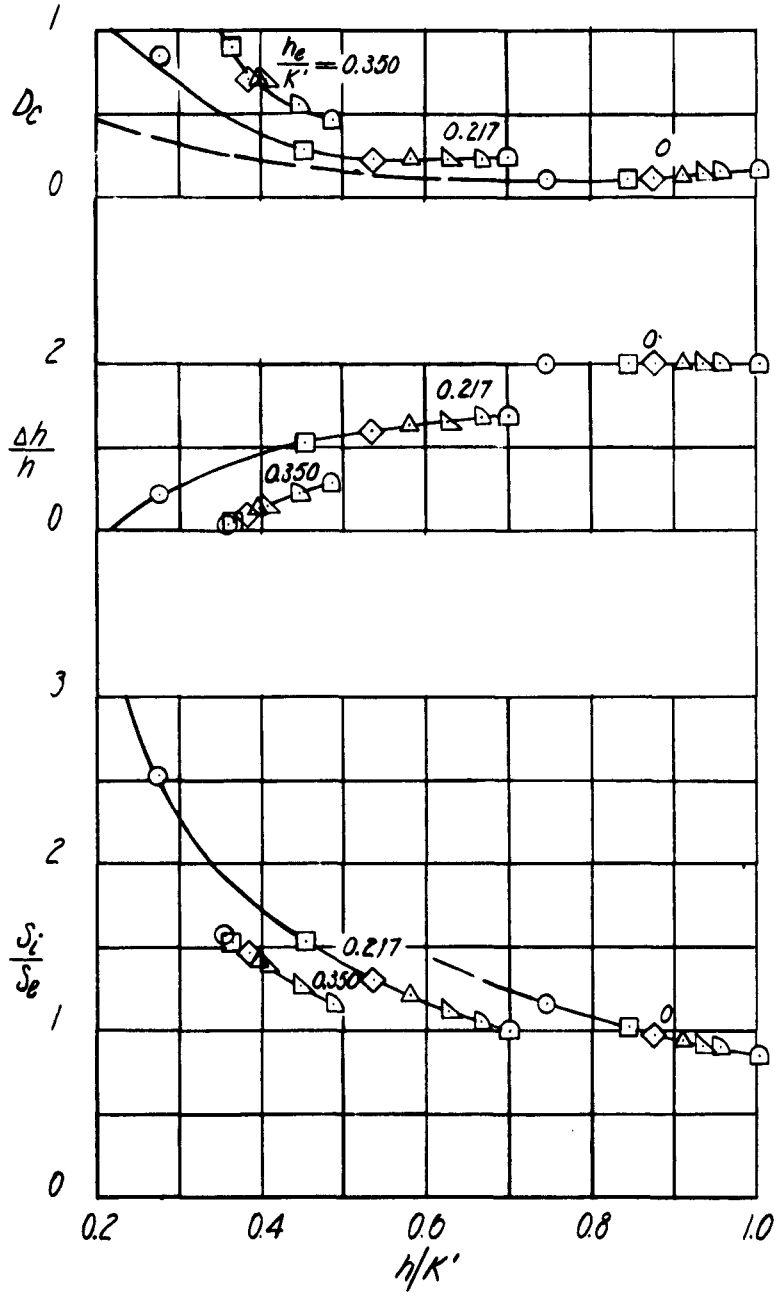

Figure 13 (Concluded)

(f) $\frac{S}{S_1} = 23.69$

FIGURE 13f

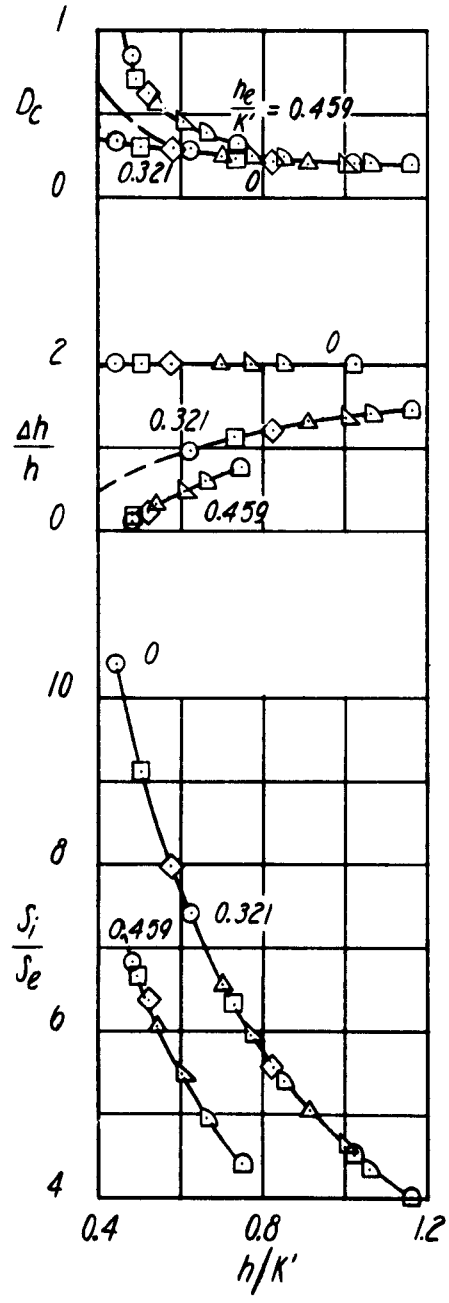

Figure 14 - Variation of the Parameters D_c, $\Delta h/h$, and S_i/S_e With h/k' for Several Values of h_e/k'. $\theta = -75°$

(a) $\frac{S}{S_i} = 5.27$

FIGURE 14a

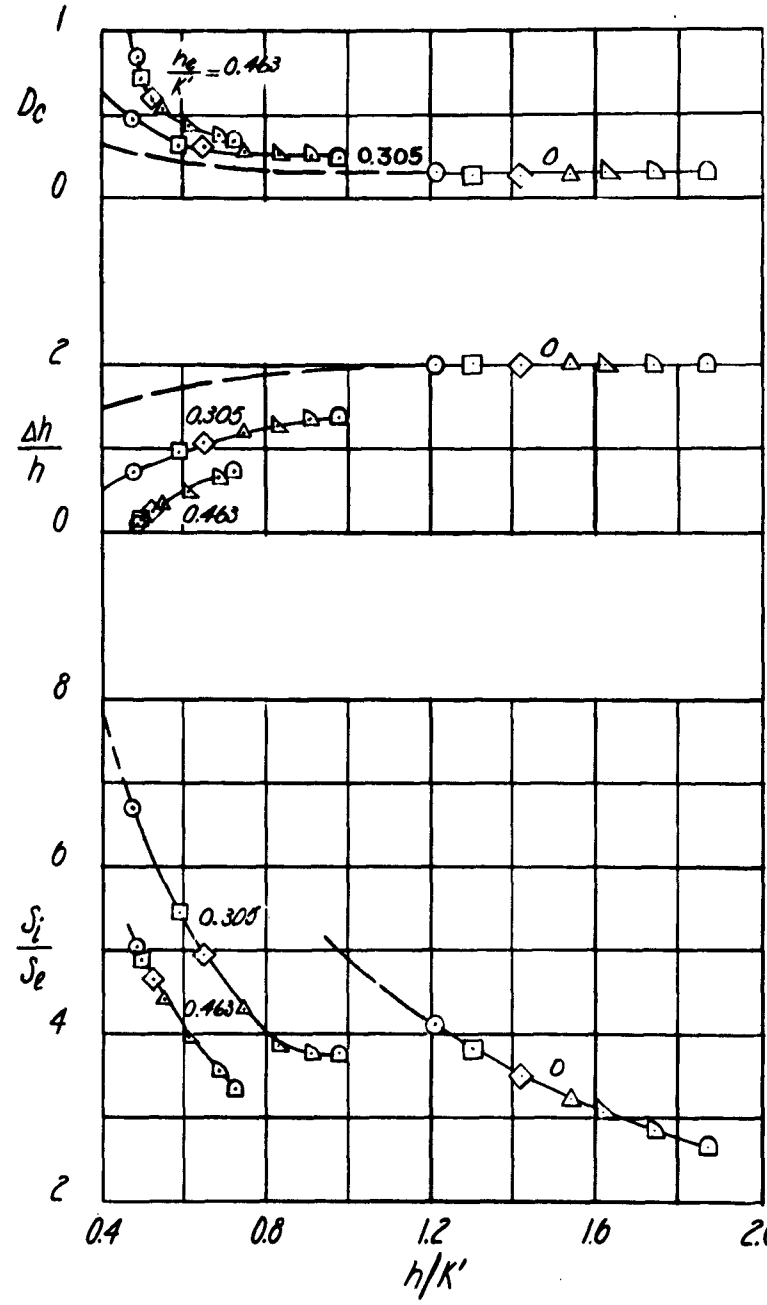

Figure 14 (Continued)

(b) $\frac{S}{S_1} = 7.17$

FIGURE 14b

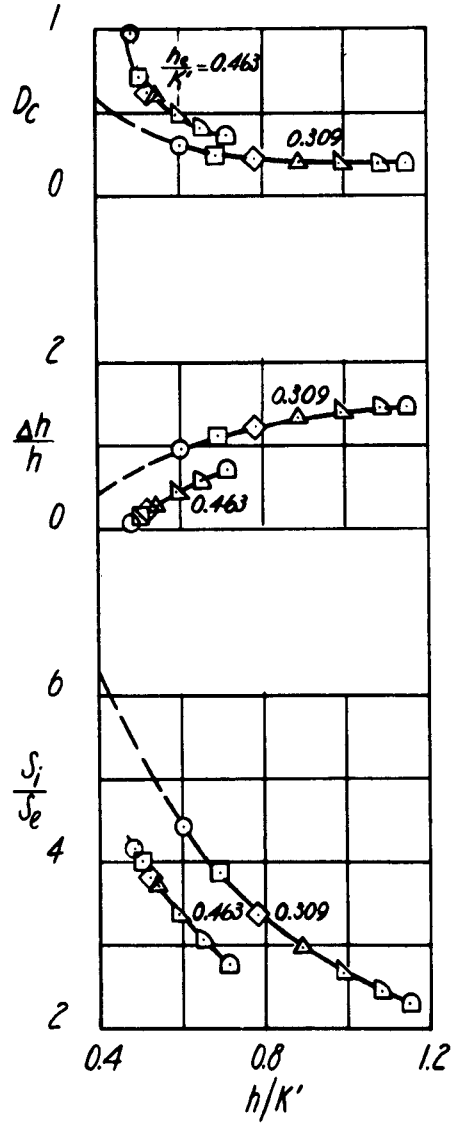

Figure 14 (Continued)
(c) $\frac{S}{S_1}$ = 8.81

FIGURE 14c

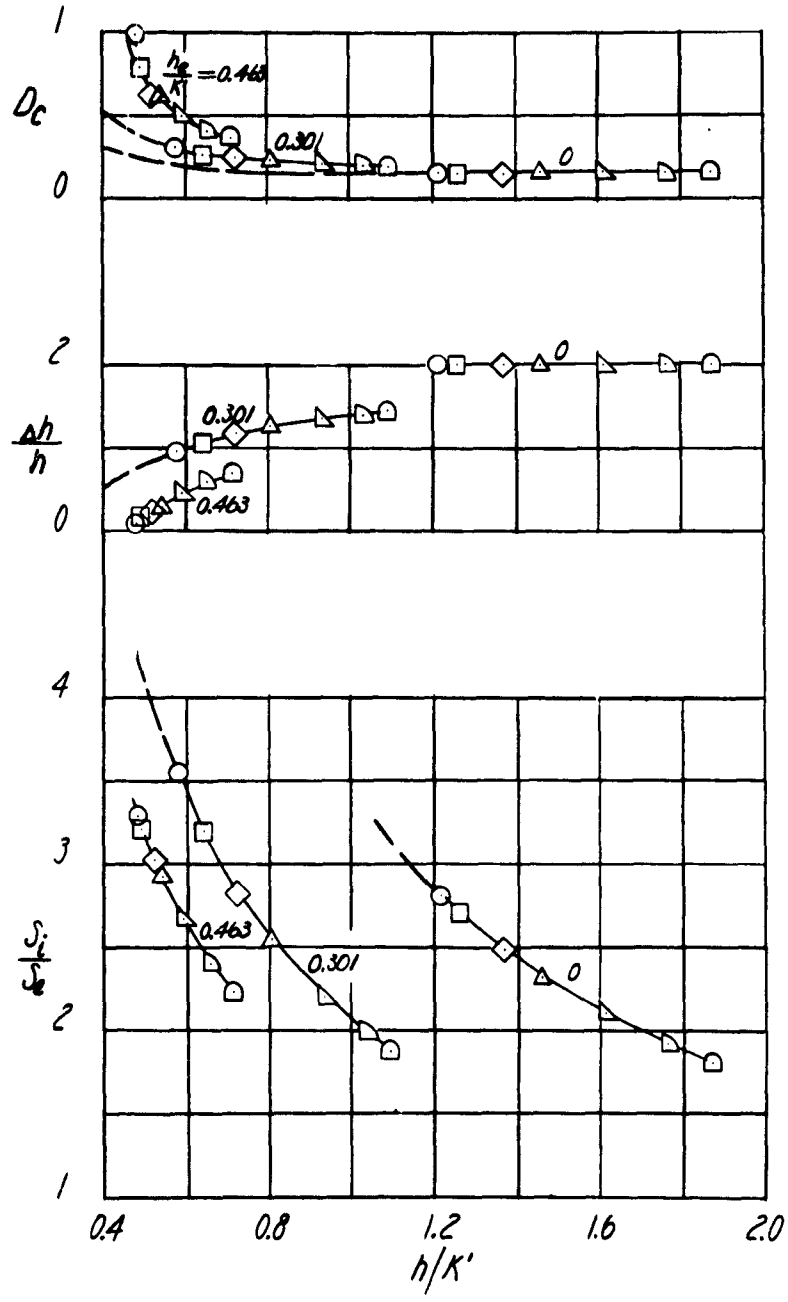

Figure 14 (Continued)

(d) $\frac{S}{S_1}$ = 11.11

FIGURE 14d

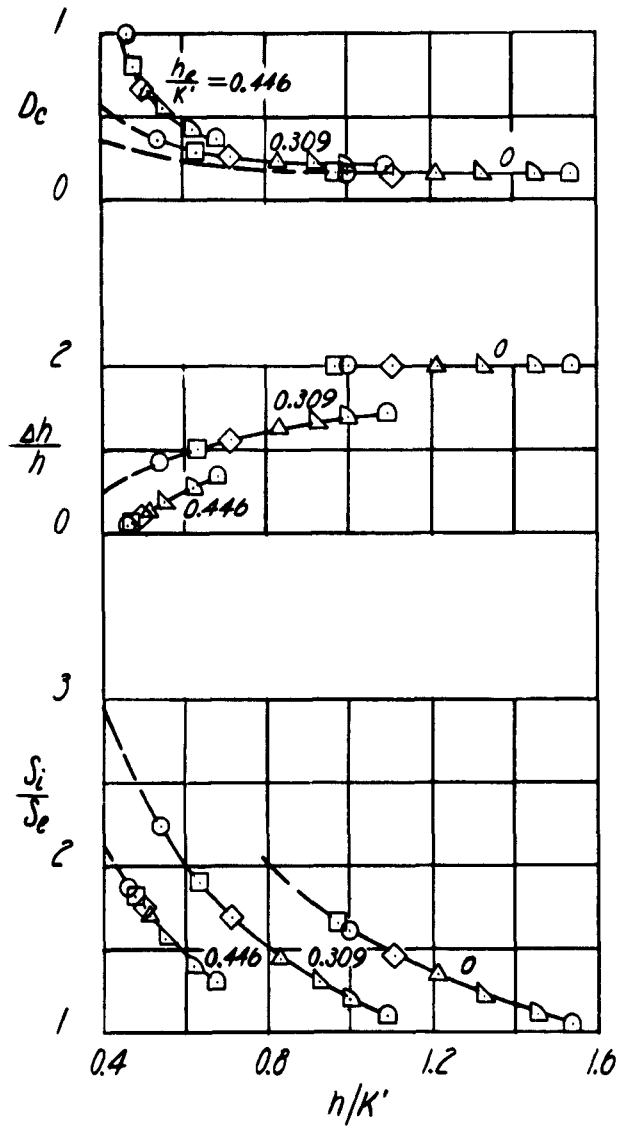

Figure 14 (Continued)
(e) $\frac{S}{S_i}$ = 15.15

FIGURE 14e

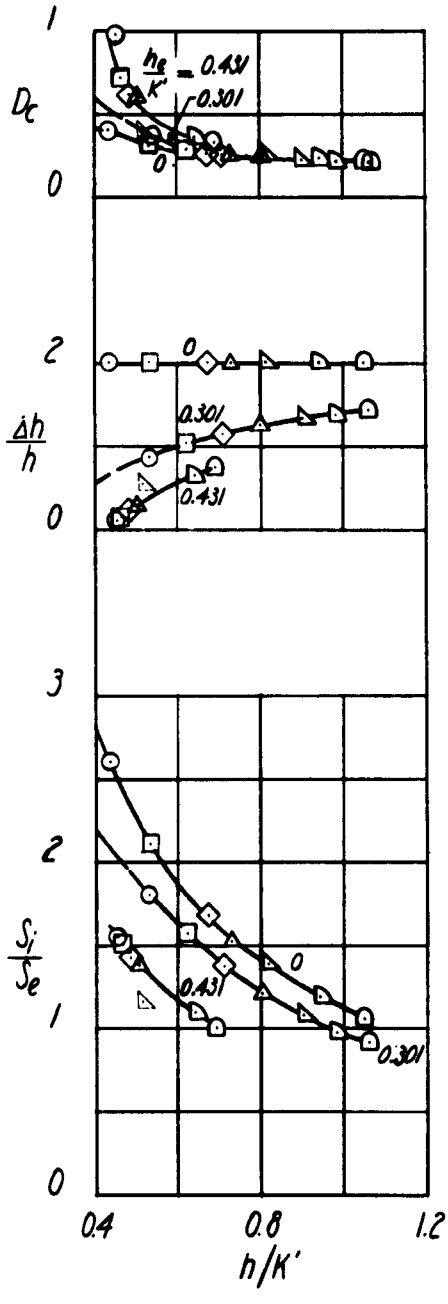

Figure 14 (Concluded)

(f) $\frac{S}{S_1}$ = 23.50

FIGURE 14f

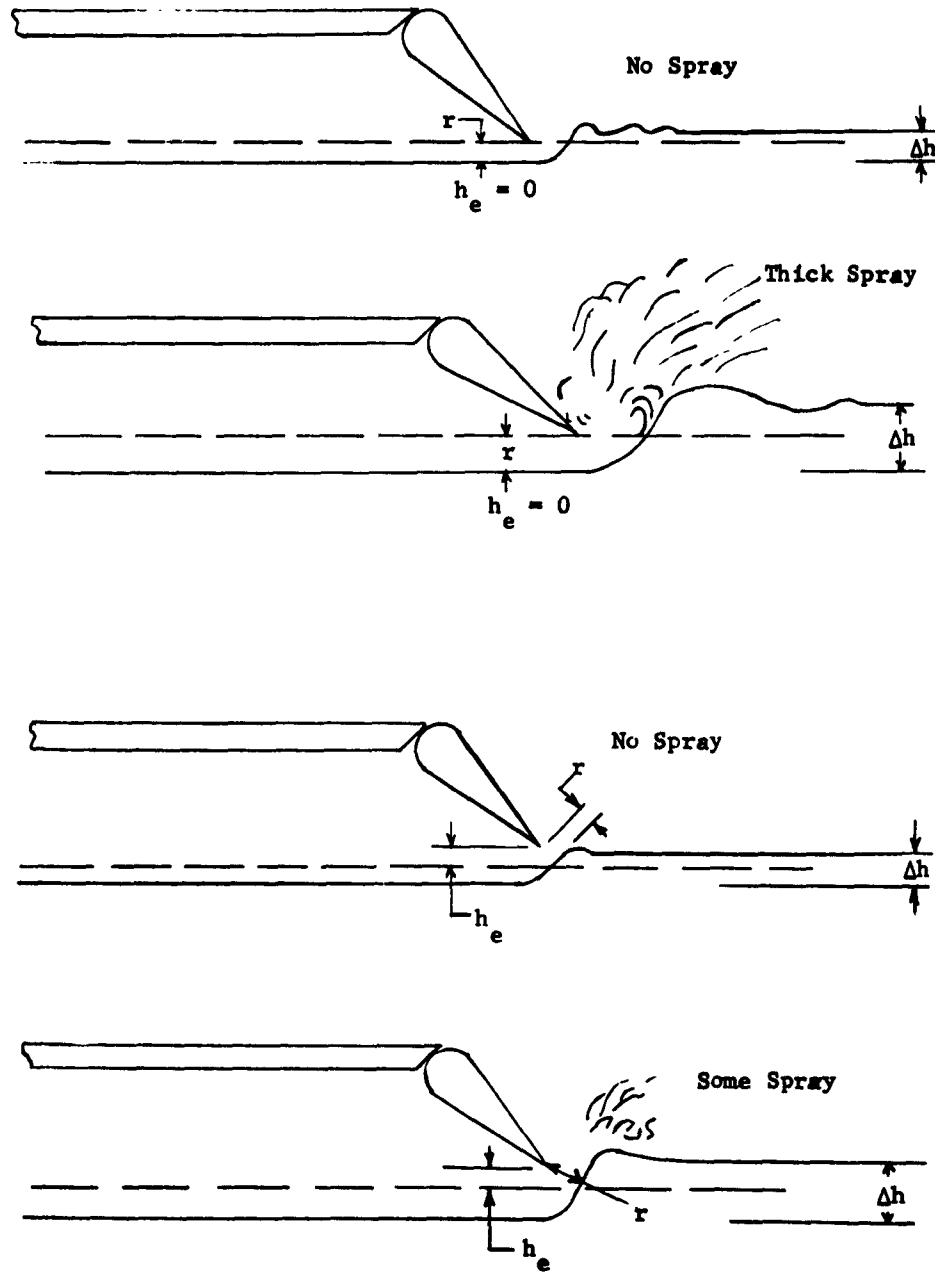

Figure 15 - General Flow Characteristics of the Trailing Edge of the Flap for High and Low Values of Δh

(a) Positive θ

FIGURE 15a

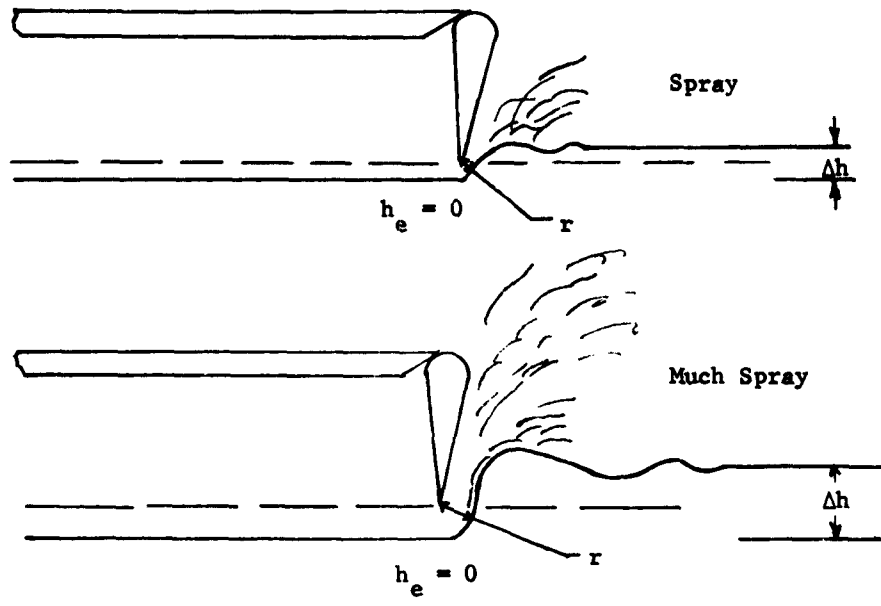

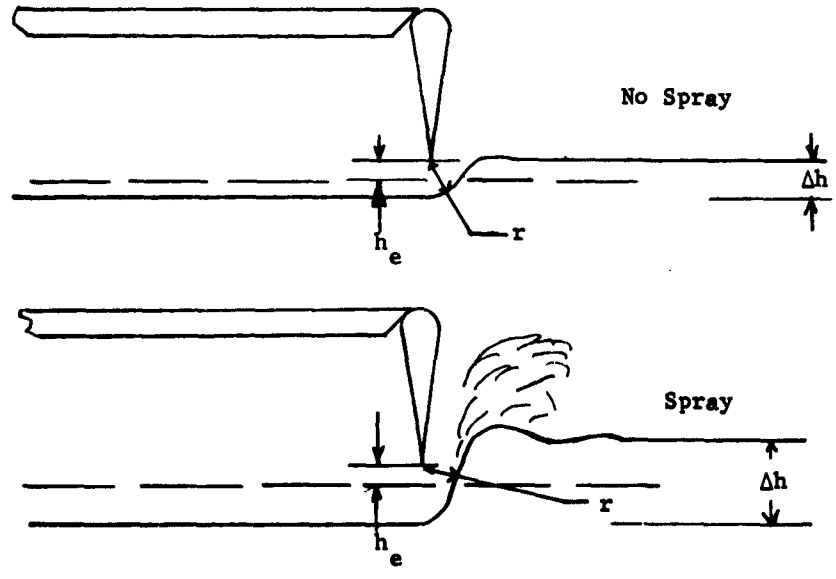

Figure 15 (Continued)
(b) $\theta \approx 0^\circ$

FIGURE 15b

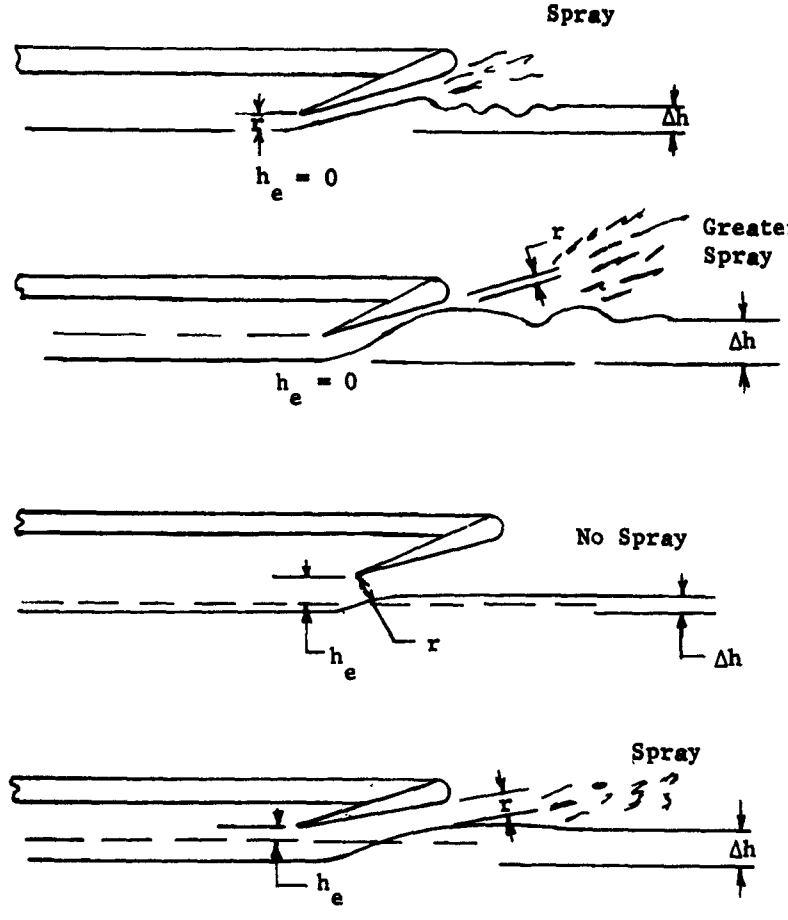

Figure 15 (Concluded)

(c) Negative θ

FIGURE 15c